

POLITECNICO DI TORINO

Corso di Laurea Magistrale in
Ingegneria Energetica e Nucleare

**Testing and modeling of a heat exchanger for
waste heat recovery in the aircraft sector**



Relatore

Prof. Marco Carlo Masoero

Candidato

Luciano Petruzzi

Dicembre 2018

List of Contents

List of Contents	1
List of Figures	3
List of Tables	6
1 Introduction	7
1.1 Context	7
1.2 Characteristics and specifications of the project	8
2 Experimental facility	11
2.1 Introduction	11
2.2 Heat exchanger	13
2.3 Hot gas circuit	15
2.3.1 Hot gas generator	15
2.3.2 Mixer	17
2.3.3 Flow straightener	18
2.3.4 Chamber	19
2.4 Water circuit	20
2.4.1 Heat to heat mode	20
2.4.2 Evaporator mode	20
2.5 Additional components	23
2.5.1 Purge system	23
2.5.2 Thermal insulation	23
2.5.3 Control panel	24
2.5.4 Acquisition system	24
2.5.5 Ducts	25
2.5.6 Support structures	26
2.6 Measuring instrumentation	27
2.6.1 Mass flowrate measuring instruments	27
2.6.2 Temperature measuring instruments	28
2.6.3 Pressure measuring instruments	30
3 Experimental results	31
3.1 Gas mass flow rate calculation	31
3.2 Uncertainty analysis	33

3.3	Thermal balance	35
3.4	Heat to heat mode	37
3.5	Evaporator mode.....	43
4	Model.....	47
4.1	Introduction.....	47
4.2	Geometry specifications	47
4.3	Heat transfer model.....	52
4.3.1	Introduction.....	52
4.3.2	Methodology: Maximum heat transfer rate and Cells division and analysis.....	54
4.3.3	Water heat transfer correlations	60
4.3.4	Comparison experimental results with numerical	61
4.4	Pressure drop model.....	62
4.4.1	Methodology.....	62
4.4.2	Comparison experimental results with numerical	69
4.5	Conclusions	71
5	Integration of the model in a Rankine Cycle.....	71
5.1	Introduction.....	71
5.2	Steam Rankine Cycle Model	71
5.2.1	Introduction.....	71
5.2.2	Pump.....	73
5.2.3	Evaporator	74
5.2.4	Expander.....	75
5.2.5	Condenser.....	77
5.3	Parametric Analysis.....	78
5.3.1	Efficiency of the Cycle.....	78
5.3.2	Electric and Thermal power produced.....	79
5.3.3	Case study: Rygge site	80
5.4	Conclusions	81
6	Conclusions and future work.....	81
6.1	Introduction.....	81
6.2	Main objectives and findings of the present study	81
6.3	Recommendations for future work.....	82
7	Bibliography	83

List of Figures

Figure 1 Configuration of a test bench [1]	9
Figure 2 Picture of an aircraft engine test bench [1]	9
Figure 3 Gas temperature along the test bench (obtained through CFD calculations)	10
Figure 4 Flow rate repartition	10
Figure 5 Hydraulic scheme of the test rig in Heat to heat mode.....	12
Figure 6 Hydraulic scheme of the test rig in Evaporator mode	12
Figure 7 Frontal and side view of the GAP 50-3-3. [2].....	13
Figure 8 GAP 50-3-3 heat exchanger side view whit the three outlet collectors [2]	14
Figure 9 GAP 50-3-3 heat exchanger assembled with the connection ducts with the two fluid flows highlighted [2].....	14
Figure 10 Test bench scheme. 1: centrifugal fan, 2: burner, 3: mixer, 4: flow straightener, 5: converging interface duct, 6: heat exchanger, 7: diverging interface duct, 8: chamber, 9: nozzle bench, 10: discharge duct. [1]	15
Figure 11 Picture of the centrifugal air fan [1]	16
Figure 12 Picture of the combustion chamber.....	17
Figure 13 Picture of mixer 1(left) and mixer 2(right) [1]	18
Figure 14 Picture of the parallel tubes flow straightener [1]	18
Figure 15 Picture of the perforated plate [1].....	19
Figure 16 Picture of the chamber.....	20
Figure 17 Picture of the nozzles(left) and the nozzles bench(right) [1]	20
Figure 18 Picture of the pump and the frequency meter.....	21
Figure 19 Picture of the Condenser.....	22
Figure 20 Picture of the tank.....	22
Figure 21 Picture of the valves for the purge system.....	23
Figure 22 Insulation material and picture of the insulated ducts. [1]	23
Figure 23 Picture of the control panel.....	24
Figure 24 Picture of the acquisition system.....	25
Figure 25 Ducts scheme. 1: straight ducts, 2: transformation pieces, 3: particular transformation pieces, 4: curved ducts. [1].....	26
Figure 26 Scheme of the type “H” support for the second level of the test bench. [1]	26
Figure 27 Picture of the volumetric flow rate counter..	28
Figure 28 Picture of the disposition of the thermocouples on the gas side.	29

Figure 29 Pictures of thermocouples type-K connected to the electronic cards(left) and the tank filled with water and ice with thermocouples immersed in(right).....	30
Figure 30 Picture of the absolute pressure sensors.....	30
Figure 31 Pictures of the differential pressure sensors of the gas (left) and of the water(right)	31
Figure 32 Heat to heat mode: Thermal power measured (gas side vs water side).....	36
Figure 33 Evaporator mode: Thermal power measured (gas side vs water side)	37
Figure 34 Operating conditions in mode Heat to heat: gas mass flow rate vs supply temperature of the gas.....	38
Figure 35 Operating conditions in mode Heat to heat: gas mass flow rate vs outlet temperature of the water	39
Figure 36 Operating conditions in mode Heat to heat: water mass flow rate vs supply temperature of the gas.....	39
Figure 37 AU vs water mass flow rate.....	41
Figure 38 Pressure drop on the gas side through the HEX vs the gas mass flow rate	42
Figure 39 Mode Heat to Heat: Pressure drop on the water side through the HEX vs water mass flow rate.....	43
Figure 40 Operating conditions in mode Evaporator: gas mass flow rate vs supply temperature of the gas.....	44
Figure 41 Operating conditions in mode Evaporator: gas mass flow rate vs outlet temperature of the water	45
Figure 42 Operating conditions in mode Evaporator: supply water pressure vs overheating	46
Figure 43 Mode Evaporator: Pressure drop on the water side through the HEX vs water mass flow rate.....	46
Figure 44 Pic of the plate with the two different chevron angles highlighted.	48
Figure 45 Scheme: simplified frontal section of the heat exchanger.	48
Figure 46 Scheme of the equivalent frontal section of the heat exchanger.....	49
Figure 47 Scheme of the cross section of the HEX with the main geometrical dimensions. ...	50
Figure 48 Flow chart representation of the algorithm	53
Figure 49 Schematic representation of the temperature profile of the two fluids inside the heat exchanger	56
Figure 50 Schematic representation of an internal pinch point	57
Figure 51 Heat to heat mode: Parity plot of the heat transfer rate (simulation results vs. experimental data).....	61
Figure 52 Evaporator mode: Parity plot of the heat transfer rate (simulation results vs. experimental data).....	62

Figure 53 Heat to heat and Evaporator mode: Parity plot of the gas pressure drop(simulation results vs. experimental data).	70
Figure 54 Heat to heat mode: Parity plot of the water pressure drop(simulation results vs. experimental data).....	70
<i>Figure 55 Hydraulic scheme of the Rankine Cycle</i>	<i>72</i>
<i>Figure 56 Temperature-Entropy diagram of the Rankine Cycle.....</i>	<i>73</i>
Figure 57 Efficiency of the Rankine cycle vs Evaporating Pressure vs Condensing Temperature	78
Figure 58 Electric power produced vs Gas mass flow rate vs Gas supply temperature	79

List of Tables

Table 1 Inlet conditions of the recovery heat exchanger inside the chimney	11
Table 2. Sensors technical data	33
Table 3 Estimated uncertainty of the final results	35
Table 4 Geometry of the plate heat exchanger	52
Table 5 Values of b_{ij} [16]	66

1 Introduction

1.1 Context

This Master thesis project has been conducted among the Thermodynamic Laboratory of the University of Liège, Belgium, in the contest of the project GREEN.

The project GREEN is a partnership between the University of Liège, CENCO, a company specialized in design, manufacture, installation of aircraft engines test benches, and ACTE, a company that designs and produces heat exchangers.

The aim of the GREEN project is to evaluate the possibility and to investigate the solutions to recover the waste heat from the exhaust gas of the aircraft engines, when these ones are tested on appropriate test benches.

An important aspect of this project is the possibility to reduce the gas emissions in the atmosphere. The European Union (EU) has set a 20% energy saving target for 2020 (compared to 1990) and a dedicated directive on Energy Efficiency to define a set of constraining measures to help European countries reach it [1]. Furthermore, on 30 November 2016 the European Commission proposed an update to the Energy Efficiency Directive, including a new 30% energy efficiency target for 2030. Following these directives, capturing and converting heat losses into electricity or using them for heating purpose, is currently arousing much attention. This allows to reduce not only the thermal pollution, due to the direct release of hot gas into the environment, but also to reduce the fuel expenditure of the airplane engines test benches close buildings and so to reduce their emissions [2]. The hot exhaust gas contains a large quantity of pollutants CO_x , NO_x , SO_x etc. which are responsible for environmental harmful impacts such as global warming, acid rain etc. [3].

Aircraft engines are in general tested to ensure their performances and safety during normal operations. In particular, specific tests are performed: in the development phase of a new model, to check if an engine works properly at the end of the production, and to verify the repair after maintenance.

During these tests an important amount of thermal energy is wasted to the environment in form of hot exhaust gases. If recovered this energy could be used in many ways, such as the production of electricity or for heating purposes. In order to recover, recycle and convert this waste energy, a solution could be represented by placing a recovery heat exchanger in the chimney of the aircraft engine test bench.

The Joule Project has been an example of waste heat recovery for boats [4], in particular ORCs systems and steam Rankine cycle of a 500 kWel power were investigated to recover the waste heat from the diesel engines of the boats in order to reduce the fuel consumption of the engine.

In [5] a literature review about the waste heat recovery in the automotive sector was done, highlighting that the Rankine Cycle and the turbocompound represent the best solution to reduce the fuel consumption.

In this context, a reduced prototype model has been designed and manufactured by ACTE company and tested in the Thermodynamic Laboratory of the University of Liège.

The experimental campaign has been divided in two parts: single-phase tests and two-phase tests. A semi-empirical numerical model is then proposed to predict the thermal and hydraulic performances of the heat exchanger.

The model needs the experimental results to calibrate the parameters used to predict its performances on a vast field of operating conditions. A comparison between the experimental and the numeric results is presented. The heat exchanger model is then integrated in a Rankine Cycle, which performances are evaluated in terms of electricity and heat production.

This thesis is organised in four section. In the first one the experimental test facility, where the heat exchanger is tested, is introduced, describing the components, the systems and the measuring instrumentations. In the second section the main results of the experimental campaigns conducted are discussed.

According to the experimental results presented in the section two, the calibration of the mathematical model is described.

In the fourth chapter the model is integrated in a Rankine Cycle evaluating the heat recovered, the electricity and the heat produced by the cycle in a case study.

Finally, in the last section the conclusion of this work are presented and discussed.

1.2 Characteristics and specifications of the project

In order to recover the heat from the exhaust gases, the first task is the position of the recovery heat exchanger along the aircraft test bench

Two possible locations for the heat exchanger were investigated:

- At the periphery of the augmenter tube;
- In the chimney, before the acoustic baffle.

The first option is not considered, since previous studies have shown that is not feasible.

On the contrary, in the chimney, due to its large cross section, a bigger heat exchanger could be used, leading to large amount of heat recovered.

Another advantage of the larger cross section of the chimney, is the reduction of the pressure drop losses of the exhaust gas stream due to the presence of the heat exchanger.

Large pressure drop must be avoided because it could affect the performances of the aircraft engine test. Table 1 Inlet conditions of the recovery heat exchanger inside the chimney

The Figure 1 show the configuration of an aircraft engine test bench, while the Figure 2 shows a picture of it.

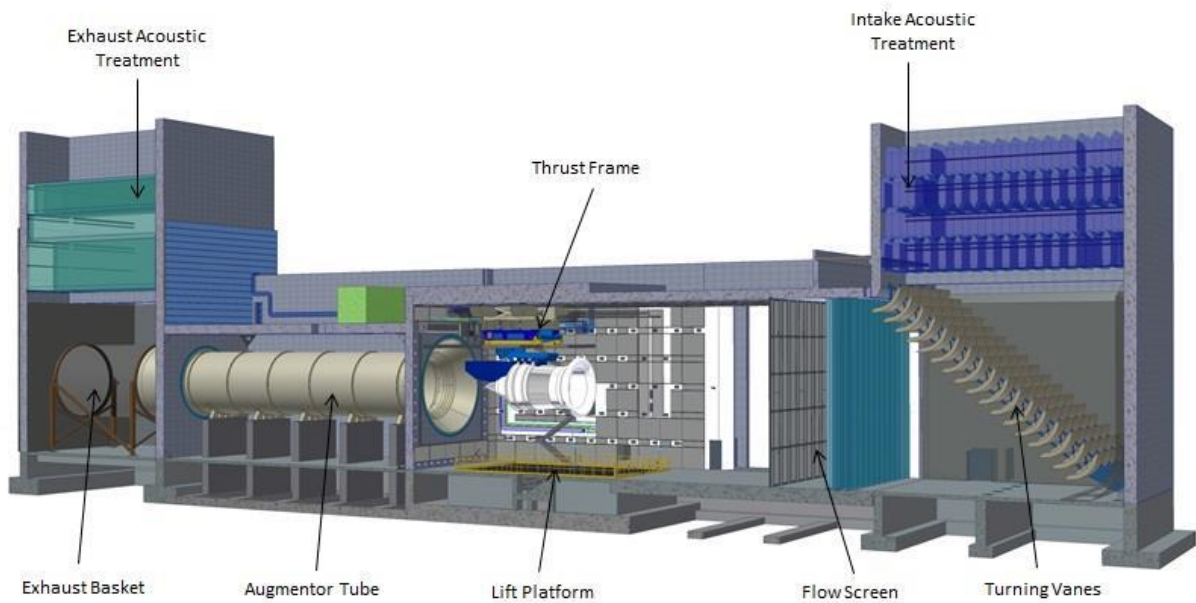


Figure 1 Configuration of a test bench [1]



Figure 2 Picture of an aircraft engine test bench [1]

From CENCO's studies the temperature of the exhaust gas in the chimney has no uniform distribution.

As shown in the Figure 3 the temperature of the gas is much higher on the right side, looking at the figure, of the chimney duct.

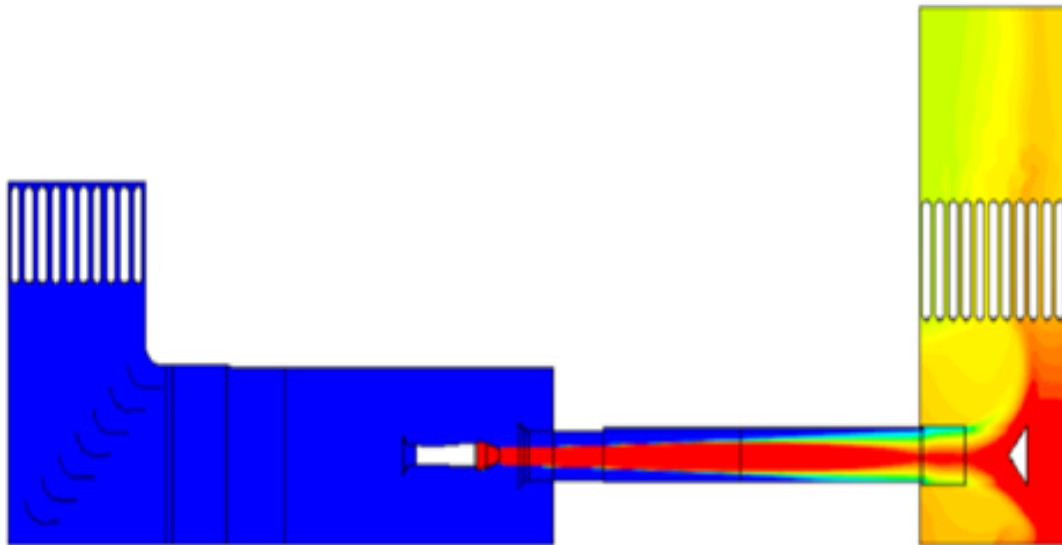


Figure 3 Gas temperature along the test bench (obtained through CFD calculations)

In addition, the gas mass flow rate is also not uniformly distributed along the section of the chimney duct.

In the Figure 4 it can be noticed how the “hot” gas in the right side consist in half of the total mass flow rate of the exhaust gas.

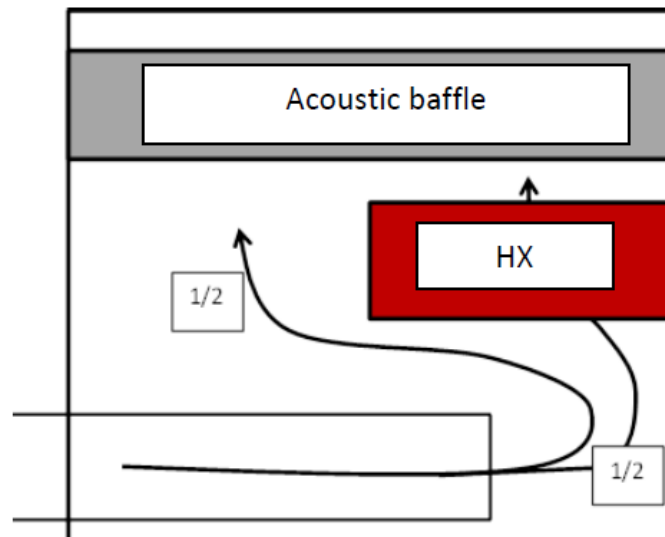


Figure 4 Flow rate repartition

Taking into account all these studies, CENCO provided the inlet conditions of the gas in the recovery heat exchanger for different sites.

In the Table 1 the mass flow rate and the inlet temperature of the exhaust gas are given, with the type of the duct that can be standard or enlarged. The mass flow rate is the one at full load operation.

Table 1 Inlet conditions of the recovery heat exchanger inside the chimney

Test bench type	Type of duct	Exhaust gas mass flow rate [kg/s]	Exhaust gas temperature [°C]
Turbofan	Standard	620	61
Turbofan	Enlarged	726.5	55
Turbojet	Standard	276	298
Turbojet	Enlarged	275.5	299
Turboprop	Enlarged	29.25	300
Turboshaft	Enlarged	17.75	317

2 Experimental facility

2.1 Introduction

In this section the experimental facility assembled at the Thermodynamic Laboratory of the University of Liège to test the heat exchanger is detailed.

The objective of the realisation of this test bench is to characterize the performance of heat exchangers to recover waste heat from exhaust gas of aircraft engines.

Since providing a mass flow rate of the gases equal to the one that can be found in the aeronautic engines is impractical and expensive, the mass flow rate is scaled.

The temperatures and the thermal power range that can be simulated is limited by the burner capacity. These ranges will be shown in the following sections.

Due to low cost, safety and high availability water is used as working fluid. The test rig is equipped with multiple sensors in order to measure the performances of the heat exchanger.

The test bench can be divided into three levels. In the first one the generation of the hot gas flow with uniform temperature is obtained. In the second level the stream is stabilized and passes through the heat exchanger, where the working fluid(water) is heated. In the third level the gas mass flow is measured and discharged at the ambient.

All the components of the test rig, with the related systems will be detailed in the following paragraphs.

The heat exchanger is tested in two modes: Heat to heat mode, water from the network is in liquid phase (Figure 5), and Evaporator mode, demineralised water in a closed loop is heated to reach overheated condition at the outlet of the heat exchanger (Figure 6).

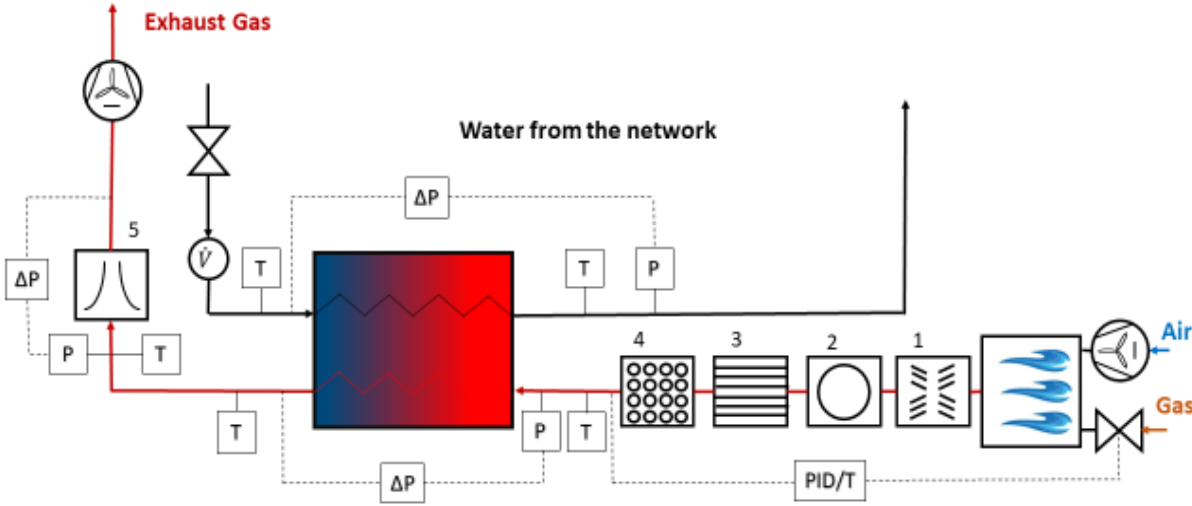


Figure 5 Hydraulic scheme of the test rig in Heat to heat mode

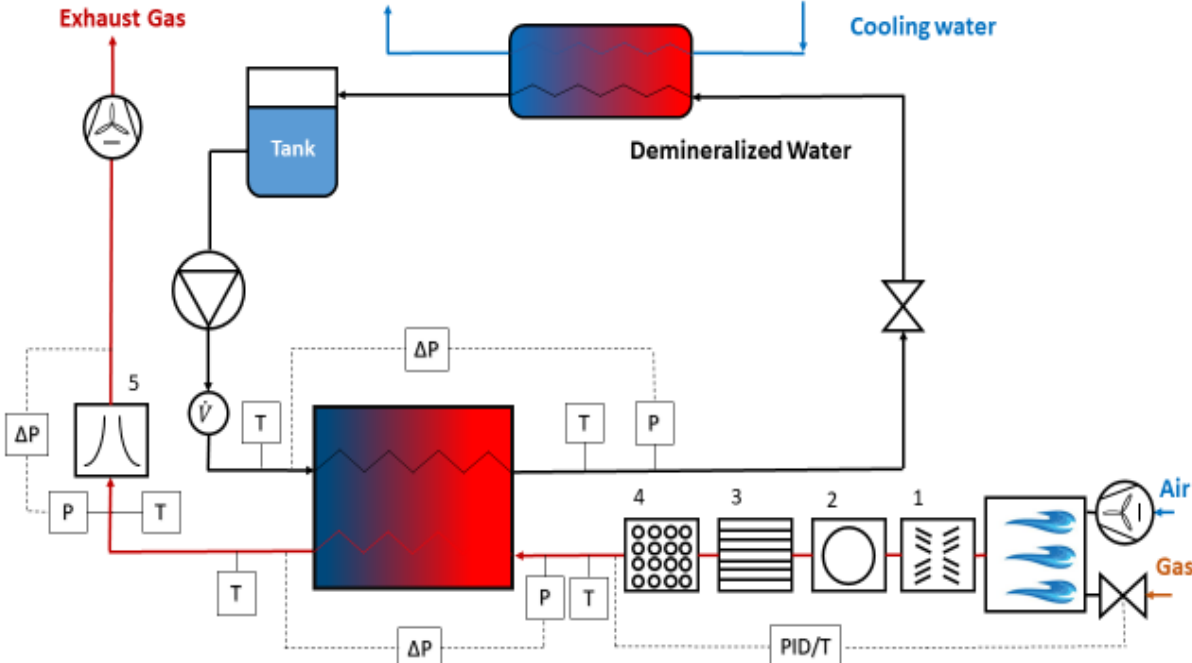


Figure 6 Hydraulic scheme of the test rig in Evaporator mode

In the previous schemes the components numbered represents:

1. the first flow mixer;
2. the second flow mixer;
3. the first flow straightener;
4. the second flow straightener;
5. the nozzles bench.

In the Figure 5 and Figure 6 the symbols T and P represents the position of temperature sensors and absolute pressure sensors respectively.

The symbol ΔP stands for the differentials pressure sensors, while \dot{V} represents the volumetric flow meter for the water.

In the next sections firstly, the heat exchanger with its main characteristics is introduced, then all the components of the bench test are described and divided in two sub-sections: the gas circuit and the water loop.

2.2 Heat exchanger

The heat exchanger is produced by the company ACTE, and the model name is GAP 50-3-3.

It consists in a counter-flow heat exchanger of a circular cross section that combine plates and pipes designed to recover the thermal heat from the exhaust gases rejected in industrial processes.

The cold fluid passes through small triangular cross section pipes laying on a rectangular plate of a length of 302 mm, made into a spiral

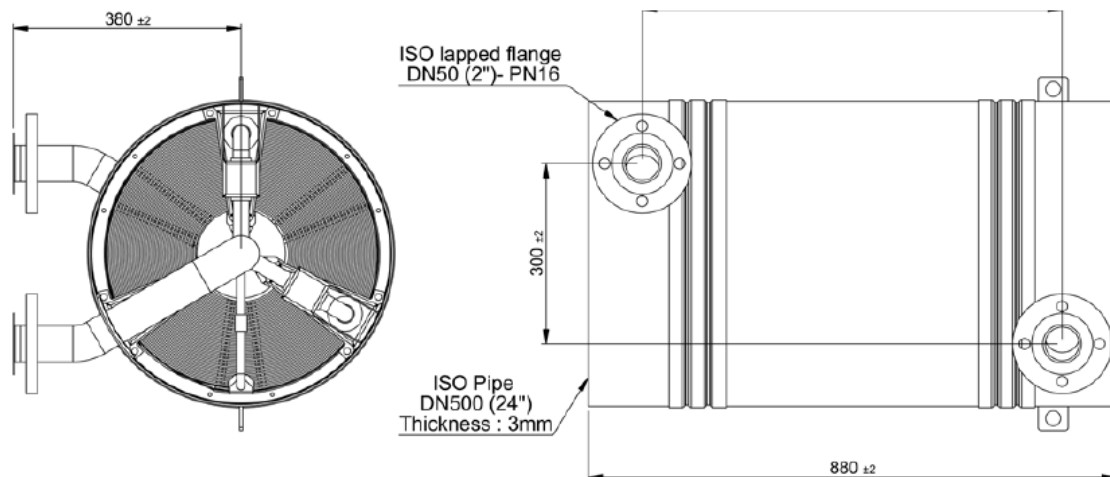


Figure 7 Frontal and side view of the GAP 50-3-3. [2]

The hot gases pass through the 3 mm gap between the tubular plates where the cold fluid goes through

The cold fluid flow is distributed at the entrance by three collectors and collected at the outlet from other 3 collectors of the same shape, as shown in Figure 8..

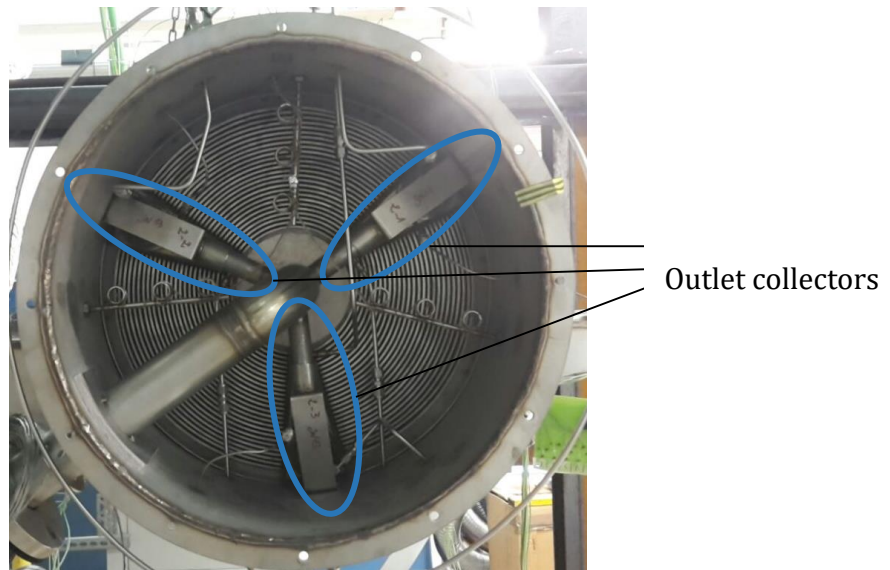


Figure 8 GAP 50-3-3 heat exchanger side view whit the three outlet collectors [2]

In the Figure 9 the configuration of the heat exchanger assemble with the exhaust gas (red arrows) ducts and the water (blue arrows) ducts on the test bench is visible.

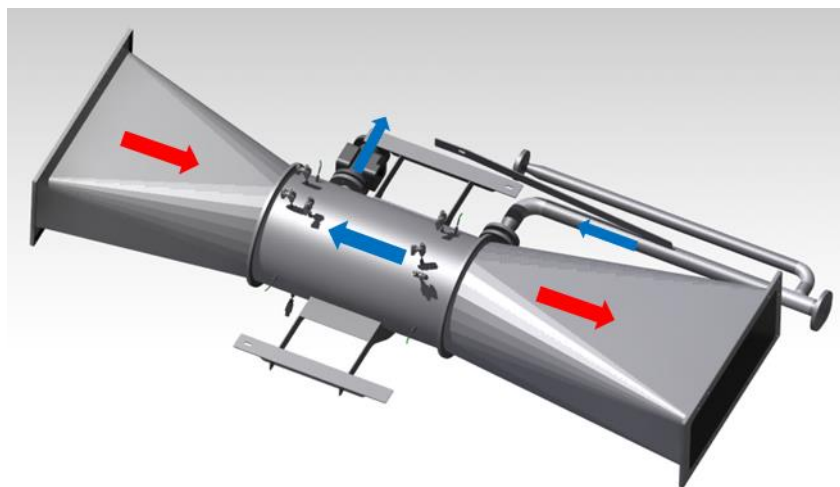


Figure 9 GAP 50-3-3 heat exchanger assembled with the connection ducts with the two fluid flows highlighted [2]

A much more detailed description of the heat exchanger with all its geometrical parameters will be done in the section 4.1.

2.3 Hot gas circuit

In this paragraph the gas stream is described component by component.

The Figure 10 represents the scheme of the test rig, enlightening all the components from the entrance of the air through the fan until it exits to the atmosphere .

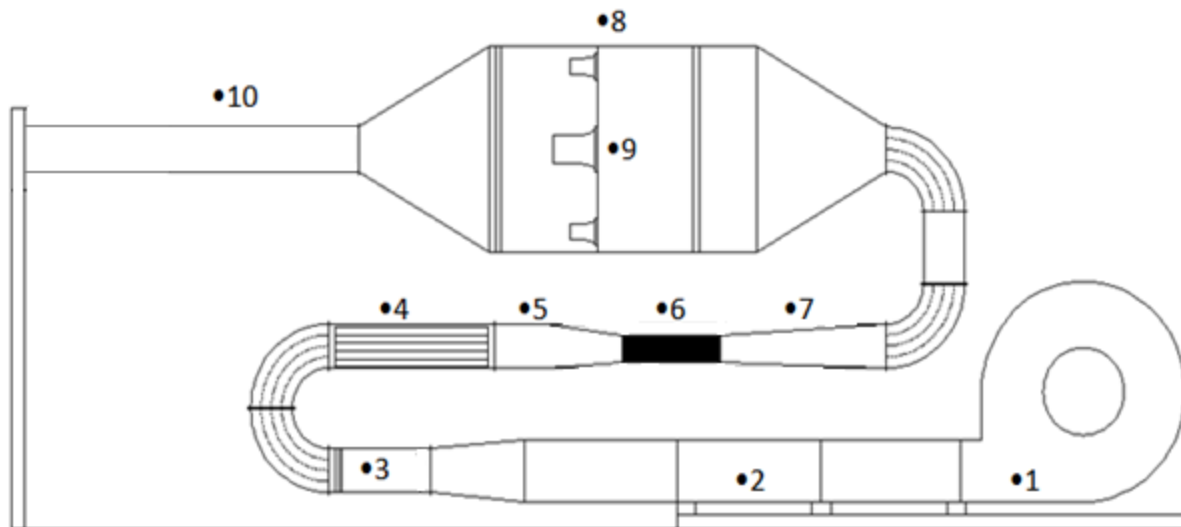


Figure 10 Test bench scheme. 1: centrifugal fan, 2: burner, 3: mixer, 4: flow straightener, 5: converging interface duct, 6: heat exchanger, 7: diverging interface duct, 8: chamber, 9: nozzle bench, 10: discharge duct. [1]

2.3.1 Hot gas generator

The hot gas generation unit is composed by:

- a centrifugal fan
- an electric motor
- a burner
- a PID control system
- gas and electrical connections

The stream of air is realised thanks to a variable speed centrifugal fan, shown in Figure 11.

It is driven by an electrical motor of 75 kW of power, equipped with a frequency drive that can modify its speed. Thanks to this it is possible to regulate and adjust the mass flow rate of the air inside the combustion chamber. The maximum mass flow rate is 4,2 kg/s for the hot gases.



Figure 11 Picture of the centrifugal air fan [1]

The air fan is coupled with a burner, that is obviously place inside a combustion chamber shown in Figure 12.

The objective of the burner is to produce hot exhaust gases from the combustion of natural gas with the air coming from the fan.

The maximum power of the burner is 450 kW, with a maximum temperature of 450 °C.



Figure 12 Picture of the combustion chamber

The hot gas generator counts a PID control system.

This system is able to control the exhaust gas temperature at the inlet of the heat exchanger varying the intensity of the flames of the burner, increasing or decreasing the power released by the burners if the temperature has to be increased or decreased respectively.

2.3.2 Mixer

In order to have an accurate temperature measurement on the gas side, stratification of the temperature along the section of the ducts has to be avoided.

Stratification is more likely to happen when a cold fluid, like air from the ambient in this case, is brought to relatively hot place like a combustion chamber at high velocity.

In this case two mixers were placed after the hot gas generator.

The design of the mixers was done by the University of Liege and it is based on mixers designs proposed by the ASHRAE (The American Society of Heating, Refrigerating and Air-Conditioning Engineers).

The first one is a static louvered mixer. It consists of fixed louvers that change the direction of the fluid stream to uniform the temperature of the fluid.

The second one consists of a metal plate with a hole in the middle. This plate canalises the hot gases in the centre, uniforming the temperature in the duct.

The mixers have been fixed inside the ducts by means of welding. They are shown in Figure 13.



Figure 13 Picture of mixer 1(left) and mixer 2(right) [1]

2.3.3 Flow straightener

To stabilize the flow, in order to perform quality tests and measurements, it is necessary to uniform not only the temperature profile, but also the velocity profile of the stream.

In general stable and uniform conditions are reached after a certain length far from the source of a disturbance. This length, called the stabilization length is directly proportional to the level of disturbance experienced by the flow.

So it means that if in a duct there is an element, like the mixer in this case, able to disturb the flow, a stabilization length before the section, where measurements take place, has to be reached to consider the stream stable.

In order to reduce the stabilization length, a flow straightener has been placed downstream the mixers.

This accessory significantly decreases eddies and rotations of the flow produced by an element of disturbance.

The type of flow straightener that has been used in the test bench is the parallel tubes type flow straightener. Flowing through the tubes the stream is forced to be straightened by the action of the tubes walls. The flow straightener design is based on a design proposed by the ASHRAE.



Figure 14 Picture of the parallel tubes flow straightener [1]

Downstream of the flow straightener a perforated plate, like the one shown in Figure 15, is placed to uniform the temperature profile.



Figure 15 Picture of the perforated plate [1]

2.3.4 Chamber

To measure the mass flow rate of the exhaust gas of the boiler a nozzles bench (Figure 17) is assembled in a chamber.

As it can be noticed in the Figure 10, the section of the chamber is much bigger than the gas ducts, this is because the flow can decelerate.

The chamber is designed respecting the standards of AMCA (Air Movement and Control Association International). The chamber is shown in Figure 16.



Figure 16 Picture of the chamber



Figure 17 Picture of the nozzles(left) and the nozzles bench(right) [1]

2.4 Water circuit

The water circuit is different in the case the tests are made in “Heat to heat” mode or in “Evaporator” mode. In the following paragraphs the water circuits are described.

2.4.1 Heat to heat mode

To test the performance of the HEX with no phase change tap water is used.

The water flows in an open circuit where the source and the sink is the network of the Laboratory. While the temperature of this water at the inlet is always around 5 to 15°C (depending on the ambient condition) and it is constant during the tests, the pressure varies from 1.5 to 2 bar (depending if the water is used from other facilities in the lab) being unstable from time to time.

Before it is returned to the network the water heated in the HEX from the hot gas, it’s mixed with cold water from the network in order to avoid perturbation of temperatures in the network.

2.4.2 Evaporator mode

During the evaporator mode the water used is demineralised water to avoid the accumulation of calcars in the HEX that can cause the obstruction of the water passage area in the tubular plates.

The circuit in this case is closed. The fluid passes through a pump, then it flows through the HEX where at the outlet of this one a thermal expansion valve is placed, then it is cooled down in a condenser and finally collected in an open reservoir.

2.4.2.1 Pump

A gear pump allows the water to circulate into the heat exchange.

Its rotational speed is controlled by a frequency meter, that allows to change the mass flow rate of the water into the heat exchanger.



Figure 18 Picture of the pump and the frequency meter

2.4.2.2 Thermal expansion valve

In the Evaporator mode the pressure of the water inside the heat exchanger is adjusted by a valve, varying the pressure between 5 and 15 bar (the maximum pressure allowed by the heat exchanger).

If a pressure bigger than 15 bar is reached the security valve releases vapour directly in the reservoir to prevent pressure conditions dangerous for the heat exchanger.

2.4.2.3 Condenser

Downstream of the valve, a condenser is placed to cool the demineralized water before it flows into the reservoir.

It is a shell and tubes heat exchanger, where the cooling is done by water from the network at 15°C.

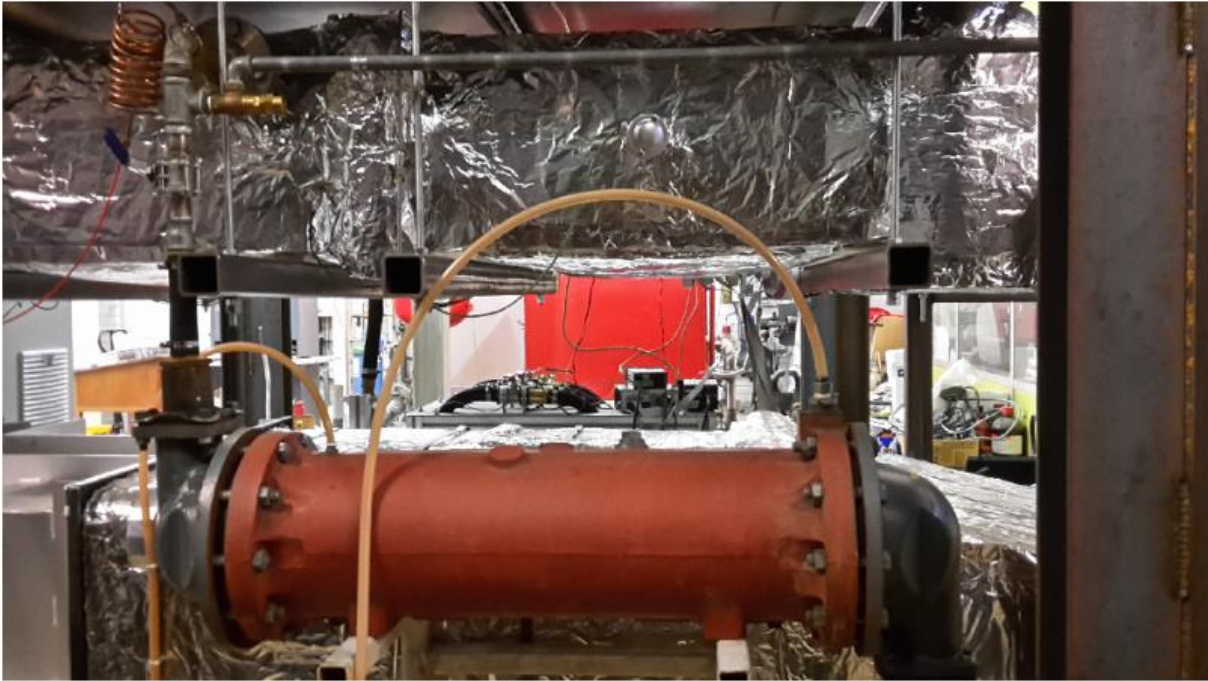


Figure 19 Picture of the Condenser

2.4.2.4 Reservoir

The reservoir is a simple tank filled by demineralized water and connected to the pump through a valve. It is an open tank where the pressure is the same as the ambient one.



Figure 20 Picture of the tank

2.5 Additional components

2.5.1 Purge system

A system of 8 valves connected with the HEX plate along its length is used at the beginning of each test session to take off the air that could be present inside the water circuit, to prevent error in the measures of the pressure and temperature sensors, and to not influence negatively the performance of the heat exchanger.



Figure 21 Picture of the valves for the purge system.

2.5.2 Thermal insulation

In order to avoid thermal losses, all the ducts on the on the gas circuit and the heat exchanger were covered with a layer of thermal insulation material.

In this case the product used was “Insulfrax” (thermal conductivity = $0.12 \text{ [W/(m}^2\text{K)]}$), a fibre material composed mostly of calcium, magnesium and silicate.

On a 50 mm layer of this, an aluminium coating was installed.



Figure 22 Insulation material and picture of the insulated ducts. [1]

2.5.3 Control panel

The start-up procedure of the boiler is done and controlled in a secure mode by means of a control panel.

Once the fan is turned on, choosing a frequency for this one, and the conditions for a safe combustion are checked, the boiler start to work.



Figure 23 Picture of the control panel.

2.5.4 Acquisition system

In order to collect the data and the measurements during the experimental test an acquisition system is used.

An Agilent card transmits the signals of the temperature and pressure sensors to the computer where the measurements are collected in .csv files, ready to be post-processed in a Matlab script.



Figure 24 Picture of the acquisition system

2.5.5 Ducts

The test bench includes three different types of ducts: straight ducts, transformation pieces and curved ducts.

The straight ducts are square, rectangular or circular sectioned ducts and they are meant to conduct the flow.

Transformation pieces are used to connect ducts with different cross section. Those pieces consist in a converging or diverging ducts.

The curved ducts are used to change the direction of the flow. These types of ducts are provided with a set of turning vanes, which are sheet metal devices used to smoothly direct the flow where there is a change of direction. The aim of the vanes is to reduce the turbulence and the resistance of the flow that crosses a changing direction duct. So, they decrease the energy loss that the flow experiments when its direction is changed.

The length of the ducts has been chosen considering the space limitations of the site where the test bench is built.

The ducts are built in regular steel and the connection between them is performed by means of flanges. The seal between ducts is ensured by the use of bolts and a thermally stable gasket designed for operation at high temperatures.

The entire ducts layout is shown in Figure 25 where the numbers represent:

1. straight ducts
2. transformation pieces
3. particular transformation pieces. They have been directly provided by ACTE company
4. curved ducts. [1]

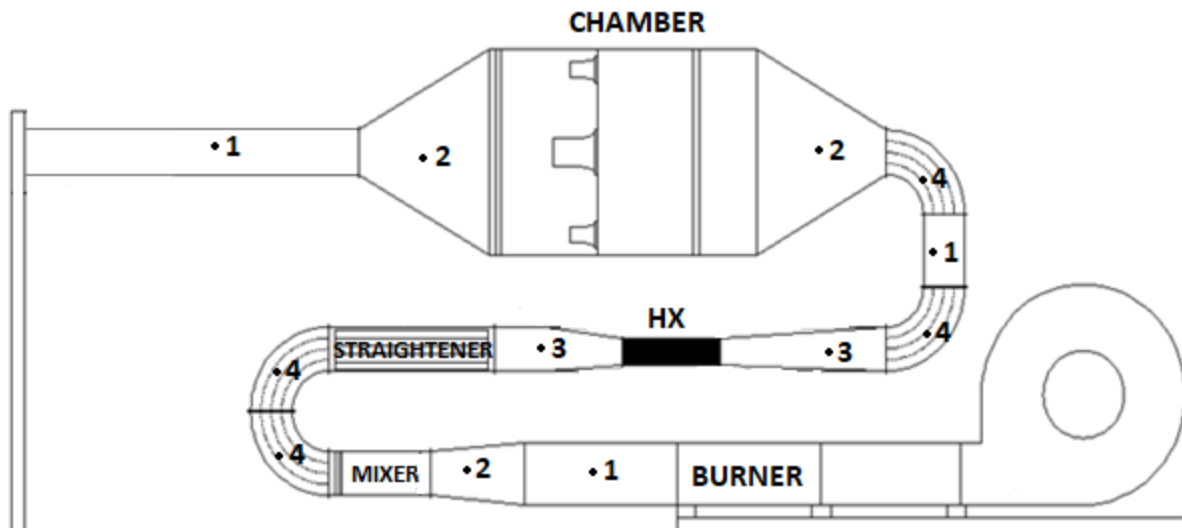


Figure 25 Ducts scheme. 1: straight ducts, 2: transformation pieces, 3: particular transformation pieces, 4: curved ducts. [1]

2.5.6 Support structures

To support the weight of the different components of the test bench, support structures have been built. The structures are able to resist the weight of the test bench components and also to provide a certain degree of freedom to avoid thermal stresses coming from the ducts dilatation.

The first type of support structure consists of a chassis built from steel profiles. This is used to support the ducts placed in the first level of the test bench.

The second type of structure consists of metallic structures that are used to support the weight of the ducts located on the first and the second level of the test bench. The mentioned structures have the shape of an "H", as shown in figure 48.

The structures are bolted to the ground and the ducts are free to glide over the structure, avoiding thermal stresses.

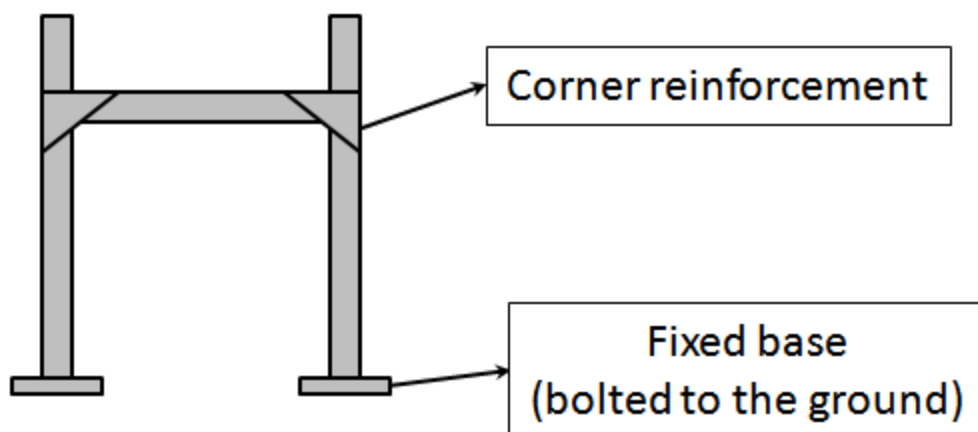


Figure 26 Scheme of the type "H" support for the second level of the test bench. [1]

The third level of the test bench is hanging and its weight is supported by chains. The chains have been attached to a set of support beams that have been installed in the room where the test bench has been built.

To increase the safety of the test bench, an additional set of metallic frames were built under the main structure of the chamber, stopping it to fall in case of failure of the suspension system. This second set of frames is also used to support part of the structure of the second level.

An extraction system has been implemented in the test bench, in order to allow the extraction of the heat exchanger. The system affords to slide the heat exchanger out of the test bench through metal guides [1].

2.6 Measuring instrumentation

As shown in the figure, three type of sensors were placed on the bench test:

- Mass flow rate sensors
- Thermocouples
- Pressure sensors

The precision and the range of each sensor will be shown in the table Table 2 at the section 3.2.

2.6.1 Mass flowrate measuring instruments

The volumetric flow rate of the water is measured by a volumetric water counter placed before the heat exchanger.

Concerning the measurement of the gas flowrate a bench of nozzles was installed inside a chamber after the heat exchanger. In this component thanks to the measure of the pressure drop before and after the nozzle, it is possible to calculate the mass flow rate of the gas.

The relation between the pressure drop generated through the nozzles and the mass flow rate, as well as the design of the nozzles bench, is determined by the standard ISO 5167.

The equations used to calculate the mass flow rate of the gas will be presented in the Experimental results section.



Figure 27 Picture of the volumetric flow rate counter..

2.6.2 Temperature measuring instruments

For all the temperature measurements, thermocouples type-K were used. On the water loop two were placed to measure the inlet and the outlet temperature on the heat exchanger, while on the gas side the thermocouples were placed in three points: inlet of the HEX, outlet of the HEX and at the inlet of the chamber.

In each point were placed 9 thermocouples distributed along the section of the conduit.

The Figure 28 shows the distribution of the thermocouples on the section of the conduit at the outlet section of the heat exchanger.

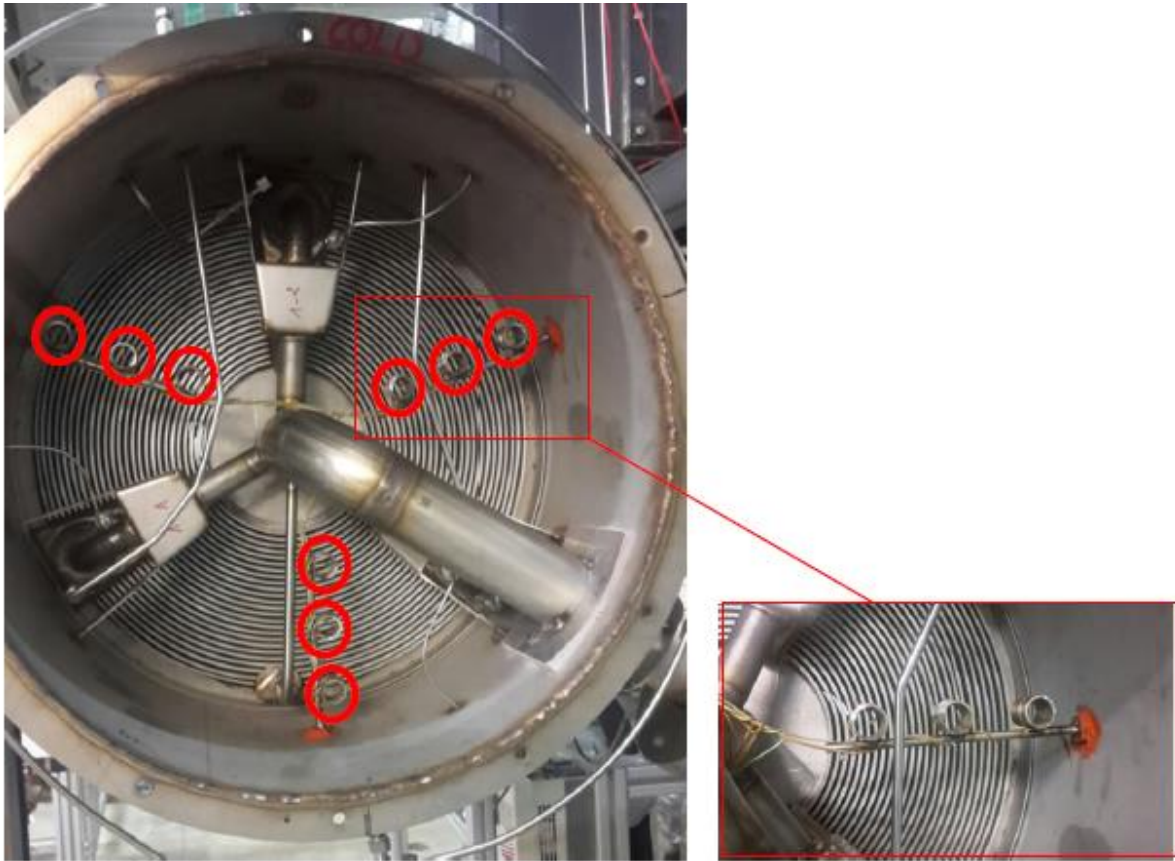


Figure 28 Picture of the disposition of the thermocouples on the gas side.

During the tests, all the thermocouples were put in contact with a cold source, made up of a little insulated cup filled of water and ice, in order to have a constant temperature reference of 0°C.



Figure 29 Pictures of thermocouples type-K connected to the electronic cards(left) and the tank filled with water and ice with thermocouples immersed in(right)

2.6.3 Pressure measuring instruments

Two types of pressure sensors are placed on the test bench: absolute and differential.

On the gas side two absolute pressure sensors are placed at the inlet of the HEX and the chamber, while on the water side it is placed at the outlet of the HEX.



Figure 30 Picture of the absolute pressure sensors

Each absolute pressure sensors is connected to a differential one in order to measure the pressure drop between two sections.

On the gas circuit two differential pressure sensors are placed (Figure 31). One measures the pressure drop on the heat exchanger, while the other one measures the pressure drop on the nozzles of the chamber.

On the water loop a differential pressure sensor (Figure 31) is placed to measure the pressure drop along the heat exchanger.



Figure 31 Pictures of the differential pressure sensors of the gas (left) and of the water(right)

3 Experimental results

In order to calibrate a model that is able to predict the performances of the heat exchanger in different conditions that the ones tested, it is necessary to perform tests in static condition.

Two experimental campaigns are conducted: in the first one water from the network is heated without reaching the saturation temperature, in the second one the goal is to have demineralized water in overheated condition at the outlet of the heat exchanger.

In this section the experimental results of the tests performed in Heat to heat and in Evaporator mode are presented and discussed.

To post-process the measurements a Matlab script has been used, calculating the thermodynamic properties with the CoolProp library.

3.1 Gas mass flow rate calculation

The procedure and the equations to calculate the mass flow rate of the gas is taken by "Laboratory methods of Testing Fans for Aerodynamic Performance Rating" ANSI/ASHRAE 51-1999 [2].

On the nozzles bench there are two types of nozzles, three "big" indicated with the subscript "G" and two "small" indicated by the subscript "P".

The letters N indicates the number of nozzles while d and A are diameter and area respectively.

Knowing that $d_G = 0.2 m$, and $d_P = 0.1 m$.

$$A_P = \frac{\pi}{4} \cdot d_P^2 \quad (3.1)$$

$$A_G = \frac{\pi}{4} \cdot d_G^2 \quad (3.2)$$

It is possible to calculate the pressure after the nozzles bench (P_{ex}) subtracting the measured pressure before the nozzles bench (P_{su}) by the measured pressure drop measured ($\Delta P_{nozzles}$):

$$P_{ex} = P_{su} - \Delta P_{nozzles} \quad (3.3)$$

As indicated in [3] the equation to calculate the mass flow rate through a nozzles bench in a chamber is:

$$\dot{m} = \sqrt{\varepsilon^2 \cdot Sum^2 \cdot 2 \cdot \frac{\Delta P_{nozzles}}{\rho}} \quad (3.4)$$

In this formula ρ is the density of the fluid, while ε and Sum are factors calculated from the following equations:

$$\varepsilon = 1 - [(0.548 + 0.71 \cdot \beta^4) \cdot (1 - r_p)] \quad (3.5)$$

$$Sum = N_{nozzles,G} \cdot Cd_G \cdot A_{f,G} + N_{nozzles,P} \cdot Cd_P \cdot N_{nozzles,P} \quad (3.6)$$

r_p is the ration of the outlet and the inlet pressure:

$$r_p = \frac{P_{ex}}{P_{su}} \quad (3.7)$$

In the case of a chamber the expansion factor β is equal to 0, while the energy factor E is equal to 1.

To calculate the Discharge coefficients Cd , an iterative process is needed since they have a non-linear dependence on the Reynolds numbers.

Iterating whit a Newton's method on the Re number the following system of equation is solved to get the solutions:

$$Cd_P = 0.9986 - \frac{7.066}{\sqrt{Re_P}} + \frac{131.5}{Re_P} \quad (3.8)$$

$$Cd_G = 0.9986 - \frac{7.066}{\sqrt{Re_G}} + \frac{131.5}{Re_G} \quad (3.9)$$

$$Re_G = \frac{\sqrt{2}}{\mu} \cdot Cd_G \cdot d_{f,G} \cdot \varepsilon \cdot E \cdot \sqrt{\Delta P_{nozzles} \cdot \rho} \quad (3.10)$$

$$Re_p = \frac{\sqrt{2}}{\mu} \cdot Cd_p \cdot d_{f,p} \cdot \varepsilon \cdot E \cdot \sqrt{\Delta P_{nozzles} \cdot \rho} \quad (3.11)$$

Once Cd is calculated, the value of the mass flow rate is then known.

It has to be noticed that all the thermodynamic properties, like the density and the viscosity, are calculated at a pressure and temperature before the nozzles.

3.2 Uncertainty analysis

The location, range and accuracy of every measuring instrument on the test rig is listed in the Table 2.

The output of the gas differential pressure sensor is a voltage in the range of 0.25 V to 4.00 V.

To convert this value in Volt to Pascal the following equation, found in the sensor datasheet, was used:

$$\Delta P_{gas} = \left(\frac{V_{output} - 0.25 [V]}{3.75 [V]} \right)^2 \cdot FS [Pa] \quad (3.12)$$

Where V_{output} is the value in Volt measured by the sensor, FS is the full-scale value of the sensor, i.e. that maximum value measureable equal to 5000 Pa in this case.

Table 2. Sensors technical data

Sensors	Location	Range	Accuracy
Flow	Water	5 m ³ /h	± 5 % (m.v.)
Pressure	Water out	[0:20] bar	± 1.5 % (F.S.)
	Gas in	[0:1.5] bar	± 1.5 % (F.S.)
	Gas chamber in	[0:1.5] bar	± 1.5 % (F.S.)
	Difference Water	[0:0.25] bar	± 1.5 % (m.v.)
	Difference Gas	[0:0.05] bar	± 1.5 % (m.v.)
	Difference Gas chamber	[0:0.05]bar	± 1.5 % (m.v.)
Temperature	Type-K	[-270:1260] °C	± 0.5 °C

Due to the errors of the measurement sensors on the test bench, calculated parameters, such as the gas mass flow rate, are affected by the error propagation of every single variable involved in its calculation.

For a general quantity Y function of n measured parameters X_i with an uncertainty Δ_i , the characterization of the propagation errors till the final results has been obtained minimizing and maximizing the taking into account all the parameters affected by the error.

To calculate the minimum/maximum of the function the *patternsearch* function implemented in Matlab was used.

All the measured parameters with the relative errors, are grouped in two vectors:

$$X = (X_1, X_2, \dots, X_n) \quad (3.13)$$

$$\Delta = (\Delta_1, \Delta_2, \dots, \Delta_n) \quad (3.14)$$

The calculated parameters are generally expressed as a function f , so the maximum and minimum value are:

$$Y_{max} = \max(f, X, X + \Delta, X - \Delta) \quad (3.15)$$

$$Y_{min} = \min(f, X, X + \Delta, X - \Delta) \quad (3.16)$$

Then the deviations from the average value Y_{ave} are:

$$err_\alpha = Y_{max} - Y_{ave} \quad (3.17)$$

$$err_\beta = Y_{ave} - Y_{min} \quad (3.18)$$

The error is then the maximum value between the two:

$$err = \frac{\max(err_\alpha, err_\beta)}{Y_{ave}} \cdot 100 \quad (3.19)$$

In the Table 3 the error of the main calculated is listed within the range of values assumed in the tests.

Thanks to the decent choice of the measuring sensors. It was possible to obtain an adequate precision on the calculated parameters. The error of the gas mass flowrate is not negligible as high is the value calculated. This is due to the propagation of the measuring errors of the

thermocouples and the pressure sensors in the calculation process presented in the paragraph 1.1.

Table 3 Estimated uncertainty of the final results

Calculated parameter	Range	Accuracy
Thermal power	40-350 (kW)	±0.5-8.3%
Gas mass flowrate	0.5-4.2 (kg/s)	±0.2-5.1%
Inlet saturation temperature	151 - 198 (°C)	±1.1-2.4%
Reynolds number (Gas)	2700-8800	±0.4-7.7%
Reynolds number liquid (Water)	30-220	±0.2-3.2%
Prandtl number(Gas)	0.68-0.71	±1.2%
Prandtl number liquid(Water)	3.2-6.8	±1.8%

3.3 Thermal balance

The thermal power exchanged on both side, water and gas, has firstly been calculated with the following equations:

$$\dot{Q}_{gas} = \dot{m}_{gas} \cdot (h_{gas,in} - h_{gas,out}) \quad (3.20)$$

$$\dot{Q}_{water} = \dot{m}_{water} \cdot (h_{water,out} - h_{water,in}) \quad (3.21)$$

The enthalpies are calculated knowing the temperatures and the pressure at the inlet and the outlet of the two fluids.

The thermal balance of the heat exchanger could be written as:

$$\dot{Q}_{gas} - \dot{Q}_{water} - \dot{Q}_{loss} = 0 \quad (3.22)$$

Where \dot{Q}_{loss} represents the thermal losses of the heat exchanger to the ambient.

Concerning the gas, its inlet and outlet temperatures were calculated as the average of the measures of the 9 thermocouples:

$$\bar{T} = \frac{\sum_{i=1}^9 T_i}{9} \quad (3.23)$$

The balances of the thermal power measured on the water side and on the gas side, in the Heat to heat and in Evaporator mode respectively, are shown in Figure 32 and in Figure 33. The calculation of the thermal power is affected by the propagation of the measuring errors of the sensors represented by the error bar for each measured point.

As it can be noticed, the error on the gas side is much larger due to a larger error commitment in the calculation on the gas mass flow rate.

Since the difference between the thermal power on the two side is always smaller than the 5%, for the following analysis the thermal losses to the ambient are considered negligible

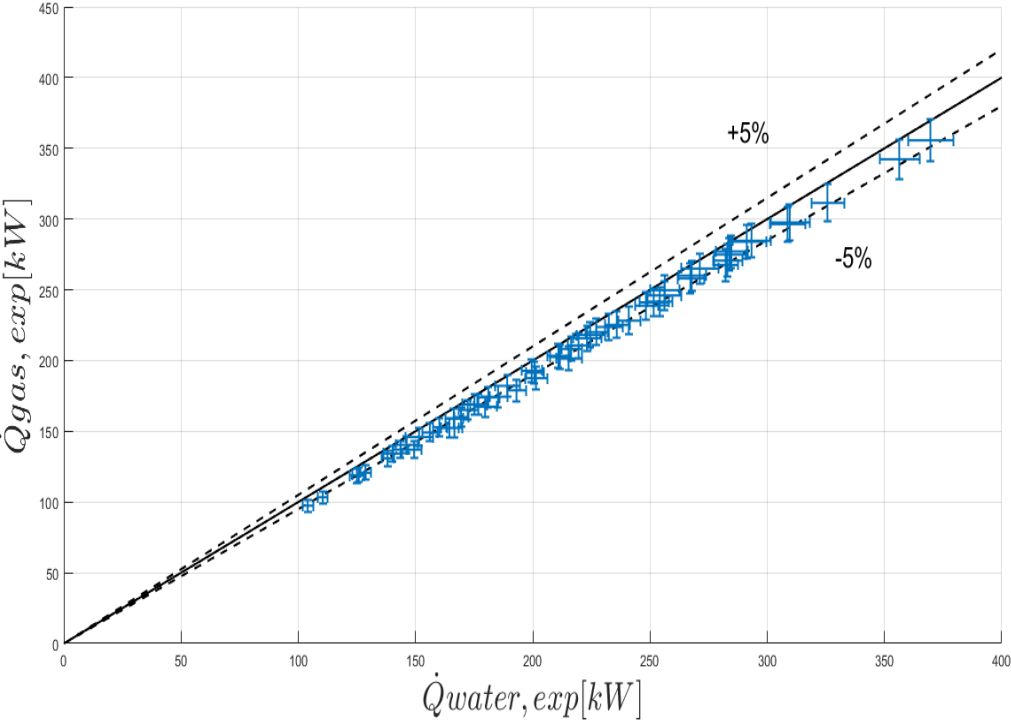


Figure 32 Heat to heat mode: Thermal power measured (gas side vs water side)

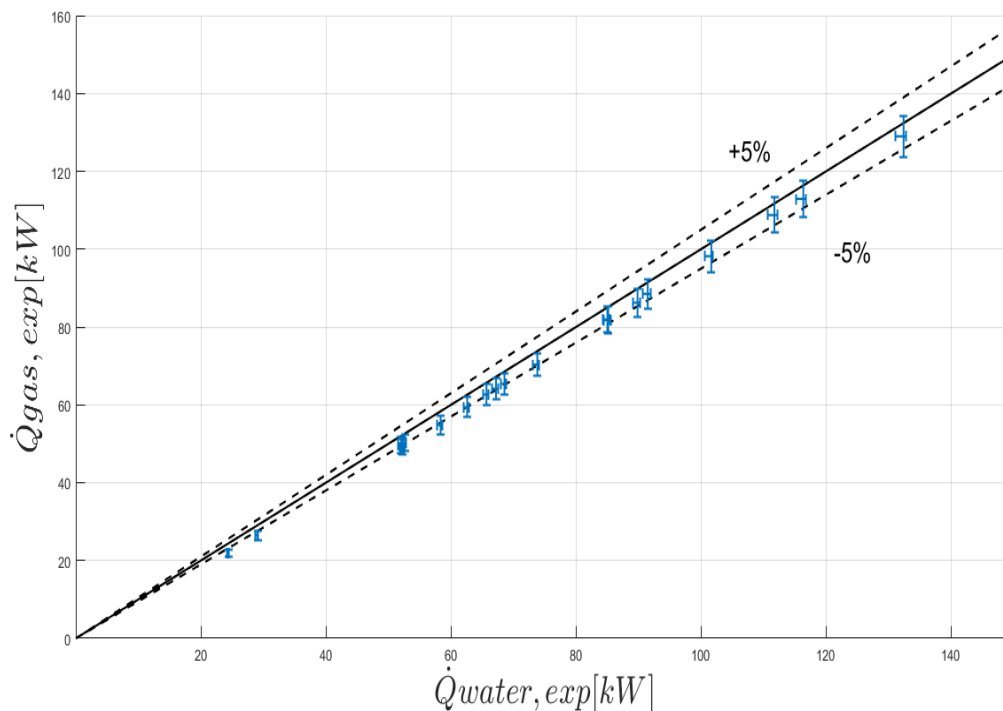


Figure 33 Evaporator mode: Thermal power measured (gas side vs water side)

Such low thermal losses are due to the thermal insulation placed all around the device.

3.4 Heat to heat mode

The starting procedure for this type of test is listed as follow:

1. Launch of the acquisition system
2. Exhaust gas fan extractor ON
3. Opening of the water flow inlet valve
4. Opening the valve of the cooling water from the network to be mixed with the hot one coming from the HEX
5. Opening the valves of the purge system
6. Start fan imposing a frequency on the control panel
7. Start boiler imposing a supply temperature for the gases

Once the boiler is started, it takes some time (~30 seconds) to check if all the condition for a safe combustion are present.

Through a PID control the burner power is regulated to reach and maintain the desired temperature of the gas at the inlet of the HEX.

In this initial phase the water flow rate is adjusted by the admission valve in order to do not have a water mass flow rate able to cool too much the gas (temperature of the gases at the outlet of the HEX > 45°C).

This is done to do not have condensation of the fumes, that could bring problems to the hydraulic conduit since this condensate is acid due to the composition of the natural gas.

Once the temperature of the gas is stable, the water flow rate is imposed in order to have a desired temperature at the outlet of the HEX.

When all the temperature and the pressure of the two fluid are stable with a maximum variation of 1 K for the thermocouples and 0.1 bar for the pressure sensor, a point of measure is obtained taking the measures every 4 seconds for at least 3 minutes.

A total of 62 stables points are obtained in a large range of operating conditions.

The three main parameters of regulation are varied in order to study their influence:

- The frequency of the boiler fan is adjusted to obtain a gas mass flow rate between 1.4 kg/s and 4.2 kg/s;
- The water flow rate is changed between 0.3 l/s to 1.15 l/s, to have an outlet temperature of the water in a range of 45°C-90 °C;
- The supply temperature of the boiler varied between 140°C to 350°C.

Two metallic plates are putted at the top and at the bottom of the burner when tests are performed with a frequency of the fan below the 30 Hz.

This is done to ensure the stability of the flame below a certain mass flow rate of the air.

Cartographies, in Figure 34 and in Figure 35, of the tests in single phase describes the range on which the measured value are varied.

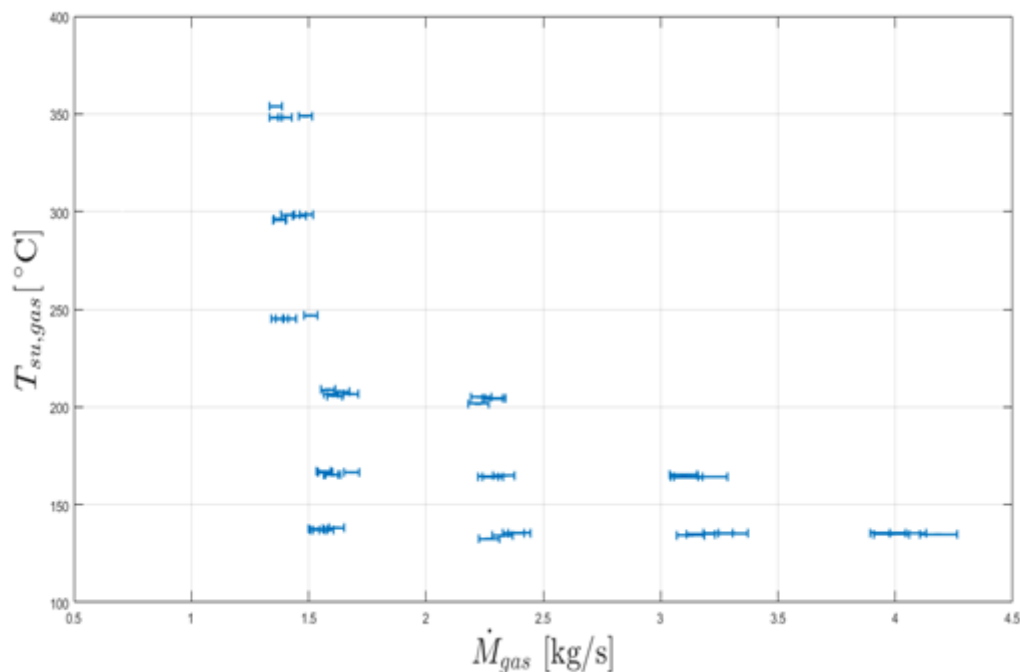


Figure 34 Operating conditions in mode Heat to heat: gas mass flow rate vs supply temperature of the gas

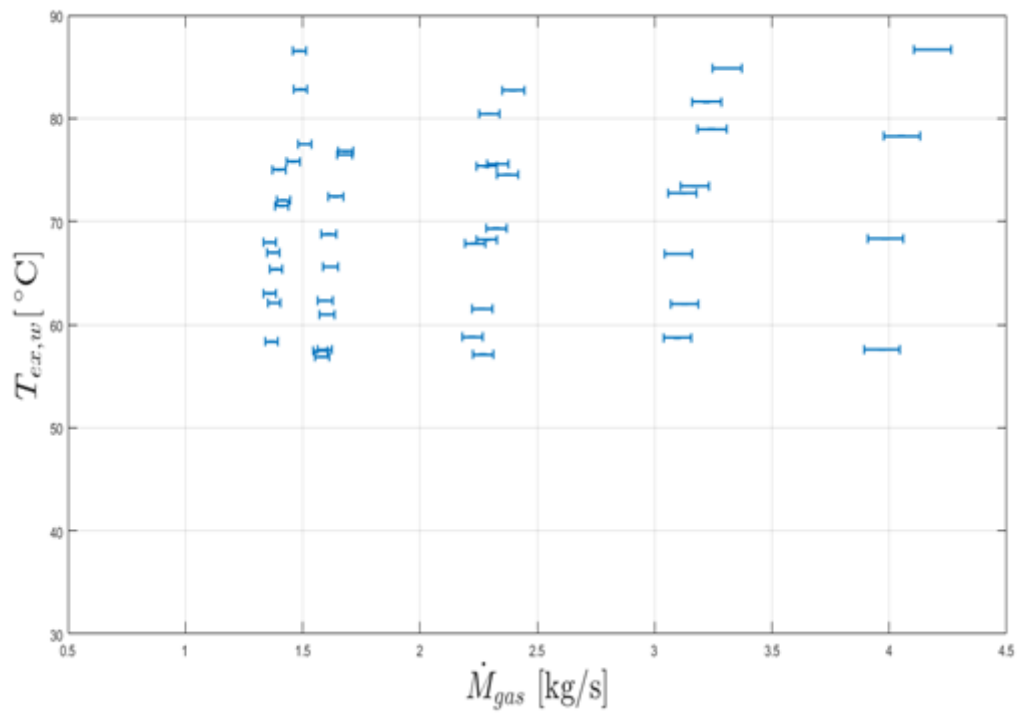


Figure 35 Operating conditions in mode Heat to heat: gas mass flow rate vs outlet temperature of the water

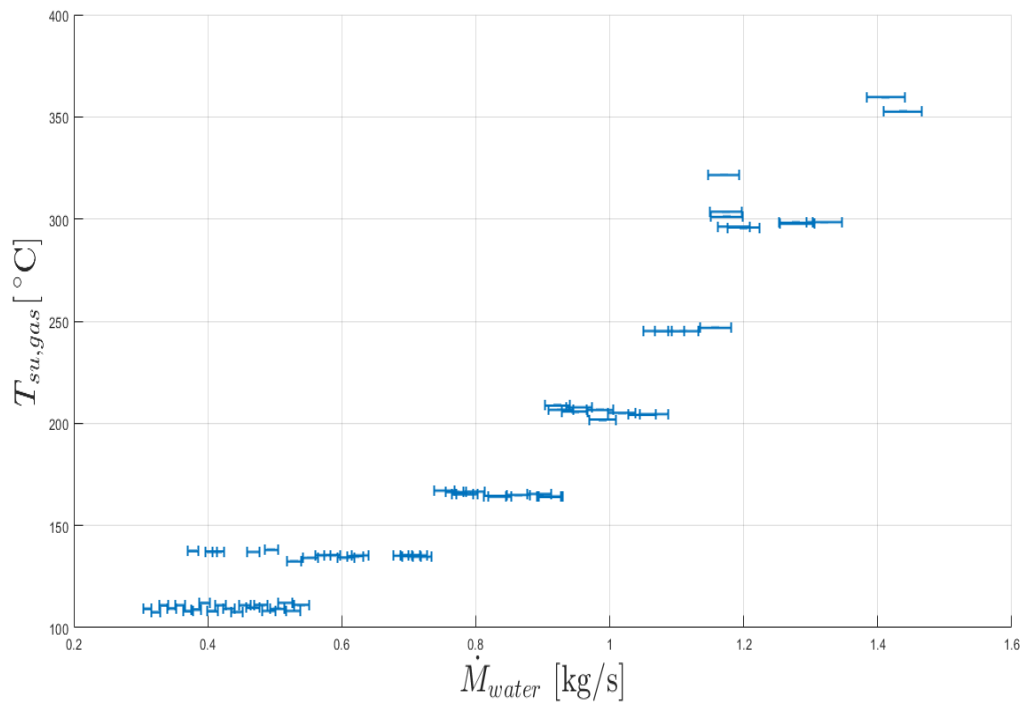


Figure 36 Operating conditions in mode Heat to heat: water mass flow rate vs supply temperature of the gas

As previously said the gas mass flow rate is imposed by choosing a certain frequency of the fan on the control panel.

The frequencies used to perform the tests are:

- 20 [Hz]
- 30 [Hz]
- 40 [Hz]
- 50 [Hz]

The imposed temperatures of the gas at the inlet of the heat exchanger are:

- 140 [°C]
- 170 [°C]
- 210 [°C]
- 250 [°C]
- 300 [°C]
- 350 [°C]

In Figure 34 it can be noticed that for a certain amount of gas mass flow rate it is not possible to reach high temperatures.

That is because the power of the boiler is limited to 450 kW, so it was not possible to increase the mass flow rate of the gas more than a certain value when the supply temperature was relatively high.

In the Figure 37 the trend of the experimental AU, i.e. the product of the heat transfer area and the overall heat transfer coefficient, against the gas mass flow rate and the water mass flow rate is shown.

Knowing that the thermal power exchanged in the HEX is equal to:

$$\dot{Q}_{HEX} = AU \cdot LMTD \quad (3.24)$$

where LMTD is the mean logarithmic temperature, equal to:

$$LMTD = \frac{\Delta T_1 - \Delta T_2}{\ln\left(\frac{\Delta T_1}{\Delta T_2}\right)} \quad (3.25)$$

ΔT_1 and ΔT_2 are the temperature difference at the inlet and at the outlet of the two fluid:

$$\Delta T_1 = T_{h,in} - T_{c,out} \quad (3.26)$$

$$\Delta T_2 = T_{h,out} - T_{c,in} \quad (3.27)$$

From the tests LMTD is known, \dot{Q}_{HEX} can be calculated with the following equation:

$$\dot{Q}_{HEX} = \dot{m}_w \cdot (h_{w,out} - h_{w,in}) \quad (3.28)$$

Finally, it is possible to calculate the experimental AU:

$$AU = \frac{\dot{Q}_{HEX}}{LMTD} \quad (3.29)$$

As expected the experimental AU is proportional to the mass flow rate of the two fluids.

It has to be noticed that the proportionality is much stronger on the gas mass flow rate. This is due to the fact that the heat transfer coefficient on the gas side is much smaller than the one on the water side because the different thermodynamic state of the two fluid.

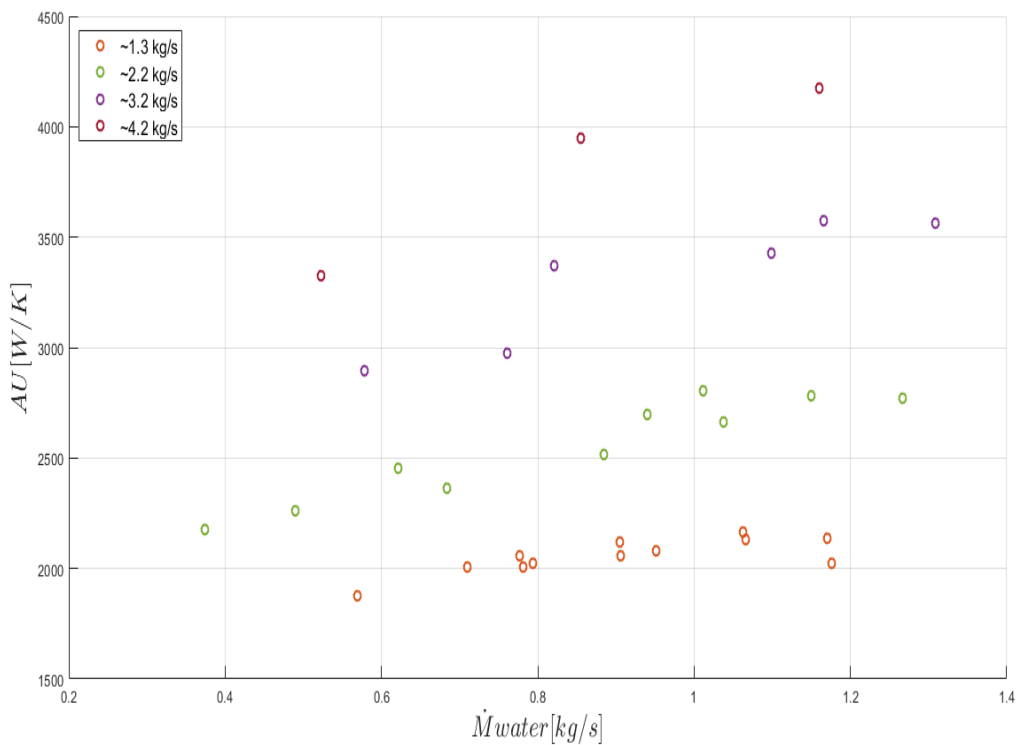


Figure 37 AU vs water mass flow rate

The pressured drop trend on the gas side and on the water side of the heat exchanger are shown in Figure 38 and in Figure 39.

It has to be noticed how the pressure drop are relatively low. This is a consequence of an adequate design of the heat exchanger. Thanks to these performances, the heat exchanger is adapted to the application investigated in this work since the low pressure drop on the

chimney of the aircraft engines test bench is a mandatory constraint that has to be taken in consideration.

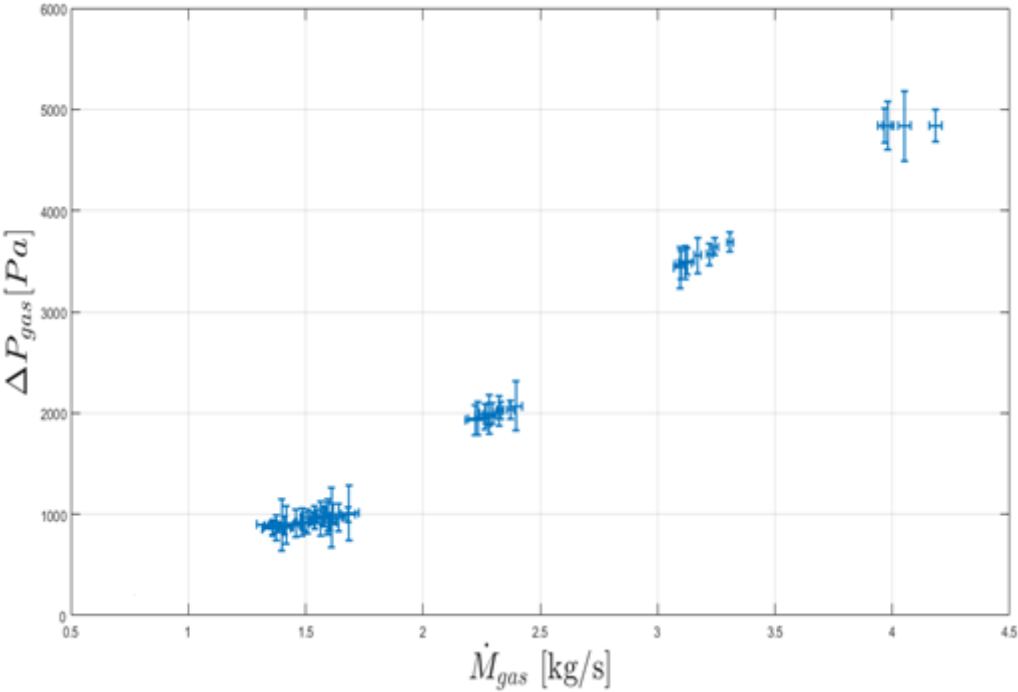


Figure 38 Pressure drop on the gas side through the HEX vs the gas mass flow rate

Concerning the pressure drop on the water side, the trend is less clear compared to the previous figure.

A reason could be found in the instability of the supply pressure provided by the laboratory network. Since many utilities are provided by the same water network, the pressure in the water network is affected by some swings.

The pressure drop measured on the water side is so low to be considered negligible in the case of the use of the heat exchange as the evaporator in a steam Rankine Cycle.

This is due to the fact that the different pressure between the inlet and the outlet does not influence the thermodynamic phenomena and condition of the fluid inside the heat exchanger

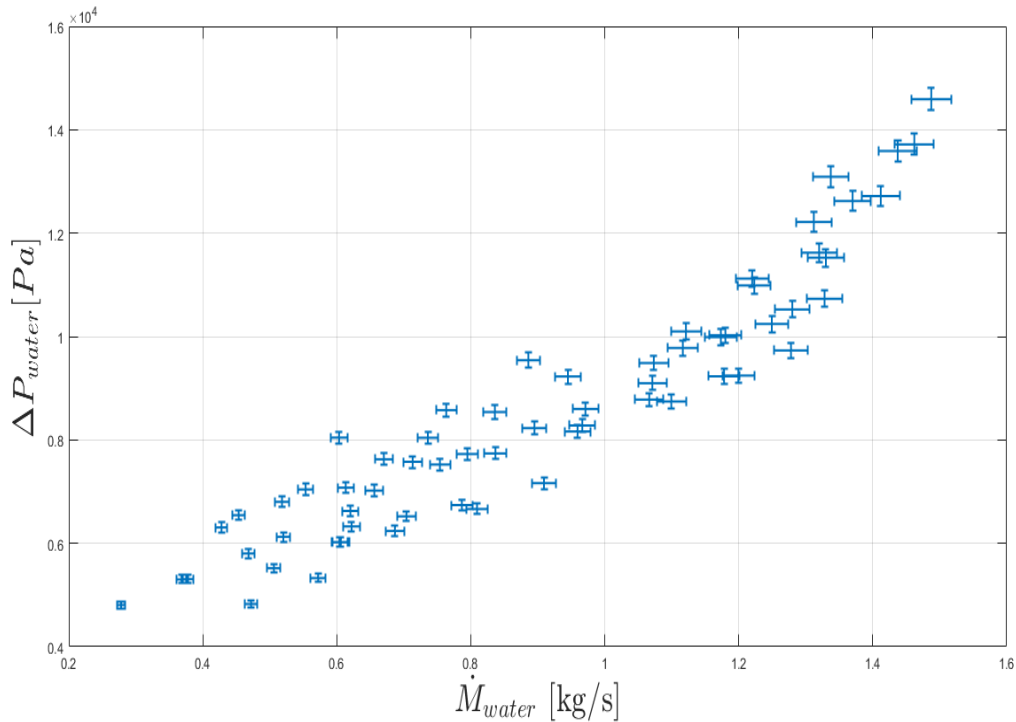


Figure 39 Mode Heat to Heat: Pressure drop on the water side through the HEX vs water mass flow rate

3.5 Evaporator mode

For the evaporator mode the starting procedure of the test varies since the water circuit changes.

The list of the steps is listed as follows:

1. Launch of the acquisition system
2. Exhaust gas fan extractor ON
3. Starting of the axial water pump at a certain speed
4. Opening the valve of the cooling water from the network that goes in the condenser
5. Opening the valves of the purge system
6. Opening of the valve gas boiler
7. Start fan imposing a frequency on the control panel
8. Start boiler imposing a supply temperature for the gases
9. Adjust the pressure of the water with bypass valve
10. Adjust overheating with the frequency of the pump

A total of 32 stable points are obtained during the experimental campaign.

The three main parameters of regulation are varied in order to study their influence:

- The frequency of the boiler fan is adjusted from 20Hz to 50Hz to have a gas mass flow rate between 0.8 kg/s and 4.2 kg/s;
- The pressure of the water is changed between 5 bar and 15 bar;

- The supply temperature of the boiler varied between 150°C to 400°C.

At a given temperature and mass flow rate of the gas, the pressure of the water is varied, and at each pressure the mass flow rate of the water is adjusted through the frequency meter of the water pump in order to obtain a stable overheating between 5°C and 40°C, as shown it is shown in Figure 40.

As for the single phase experimental campaign, the frequencies used to perform the tests are:

- 10 [Hz]
- 20 [Hz]
- 30 [Hz]
- 40 [Hz]

The imposed temperatures of the gas at the inlet of the heat exchanger are:

- 200 [°C]
- 250 [°C]
- 300 [°C]

It has to be noticed in Figure 42, that due to instability issues [4] a minimum pressure of 5 bar is maintained in the circuit.

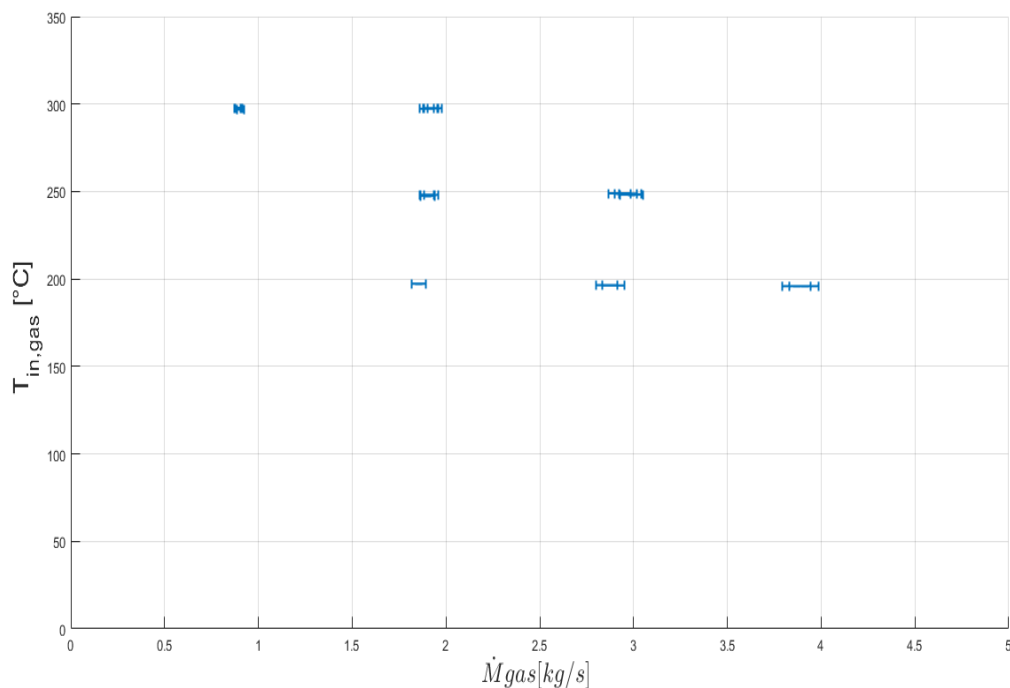


Figure 40 Operating conditions in mode Evaporator: gas mass flow rate vs supply temperature of the gas

The outlet temperature of the water is plotted against the gas mass flow rate in Figure 41.

Since some joints at the outlet conduit of the heat exchanger were not able to resist at more than 250 °C, this value was considered the limit to respect concerning the maximum outlet water temperature.

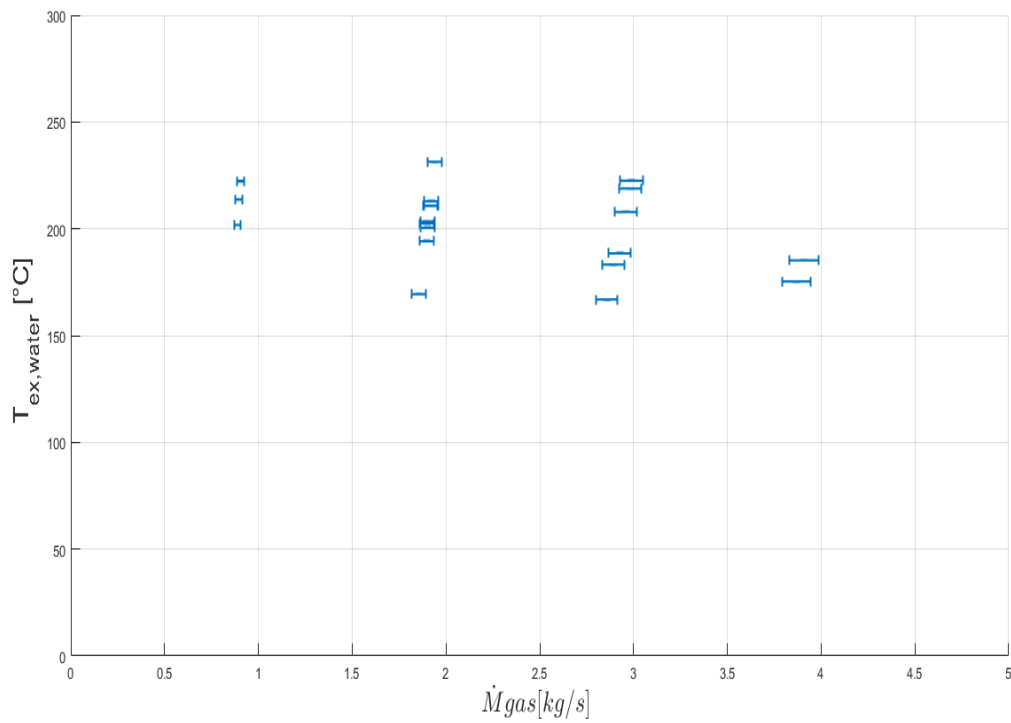


Figure 41 Operating conditions in mode Evaporator: gas mass flow rate vs outlet temperature of the water

The over-heating of the water is defined as the difference between the outlet temperature of the water and its saturation temperature, has been a difficult parameter to control during the experimental campaign.

This is mostly due to the oscillation of water pressure because of the pressure wave generated by the different velocity of the vapour compared with the liquid in the two phase region.

For a range of evaporating pressure of [5,15] bar, the mas flow rate of the water was adjusted in order to obtain different over-heating at the same pressure in a range of [10,50] K (Figure 42).

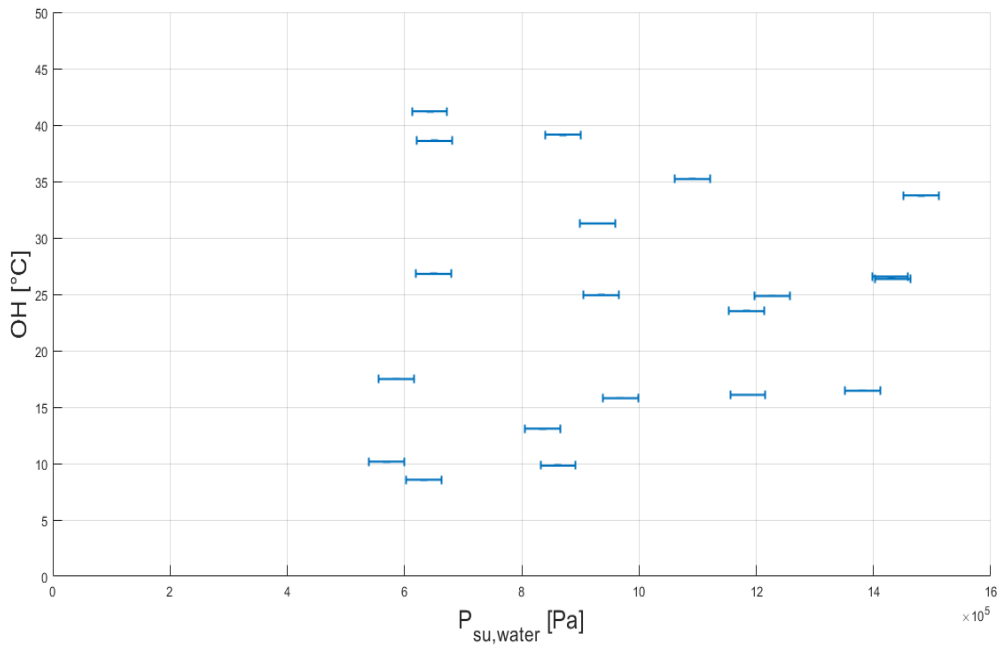


Figure 42 Operating conditions in mode Evaporator: supply water pressure vs overheating

Concerning the pressure drop on the water side, the trend in function of the water mass flow rate is quite dispersed and not clear (Figure 43).

The main reasons behind this trend are probably the fluid instability during the two-phase tests, and the lower precision of the water pressure difference sensor at such low values measurements.

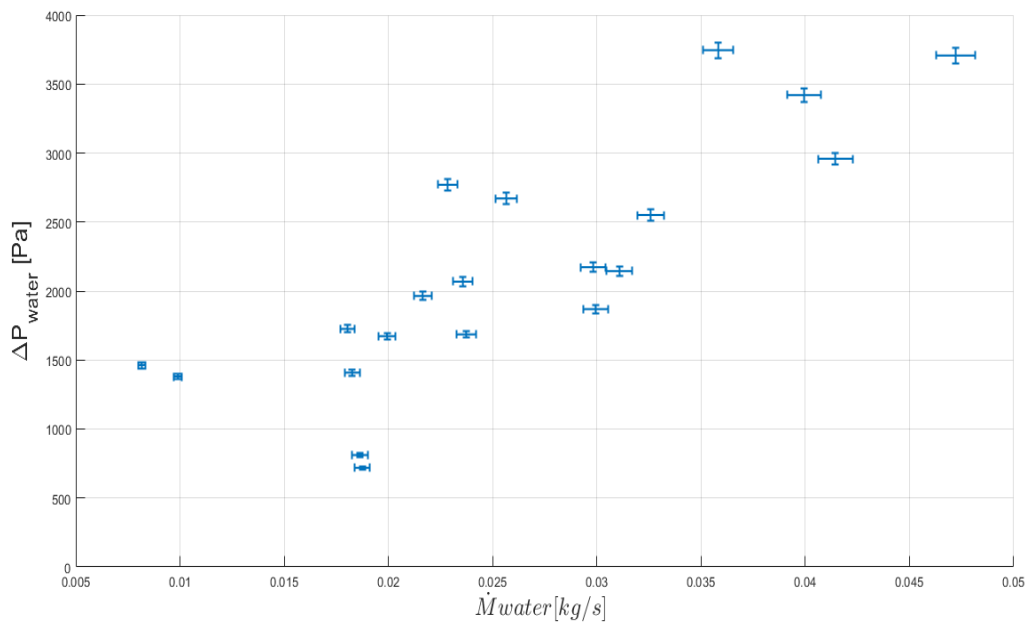


Figure 43 Mode Evaporator: Pressure drop on the water side through the HEX vs water mass flow rate

4 Model

4.1 Introduction

In this chapter the geometry of the GAP heat exchanger is presented and simplified for the calculation of the main geometrical parameters such as the hydraulic diameters of the two fluids and the heat exchange surface,

Then the numerical model is introduced explaining the calibration of the parameters, the methodology and the solution approach used.

Finally, the results obtained with the calibrated parameters are given and compared with the experimental ones.

4.2 Geometry specifications

The first step to model the hydraulic and thermal performance of the heat exchanger is represented by the calculation of the geometrical parameters.

These one are necessary to calculate the hydraulic diameter of the two fluid and the exchange surface.

The GAP 50-3-3 presents a geometry that consists in a brazed plate of 302 mm length (L_{HEX}) and 3 mm thick (s_w) rolled up in a spiral enclosed in a ring of internal diameter $D_i = 160 \text{ mm}$, and an external diameter $D_e = 455 \text{ mm}$.

The plate spiral is shaped in order to maintain a gap of 3mm between each passages, where the gas can flow.

The plate is composed of two aluminium paper welded together, where a pattern is printed to have channels of triangular shape cross section.

These channels, where the working fluid flows, follow a path inclined respect to the axial direction of the plate by an angle, named the chevron angle in these type of heat exchangers, that change in the way shown in the Figure 44.

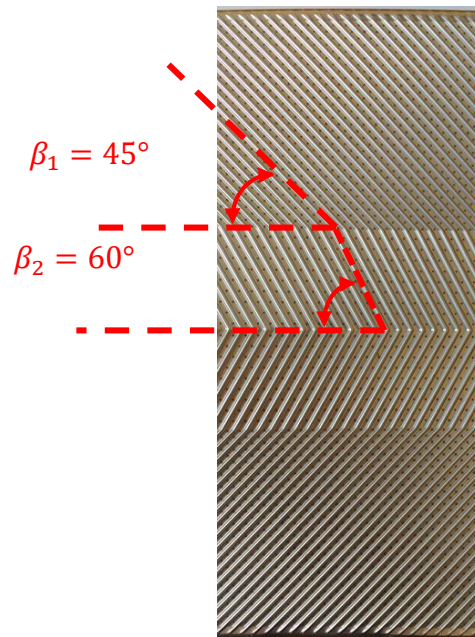


Figure 44 Pic of the plate with the two different chevron angles highlighted.

The geometry for the cross section of the heat exchanger is reduced to an equivalent frontal surface of a horizontal rectangle (Figure 46), with a thickness equal to the sum of the thickness of the aluminium plate plus the gap.

The spiral is reduced to concentric circles in order to simplify the scheme in Figure 45.

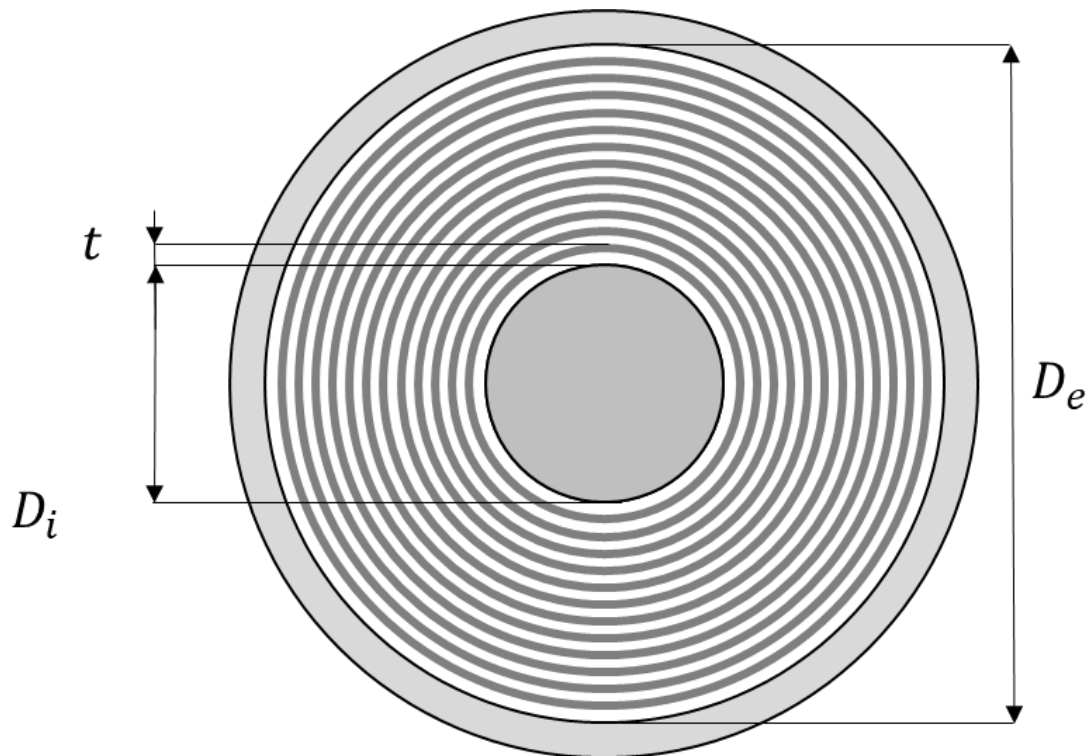


Figure 45 Scheme: simplified frontal section of the heat exchanger.

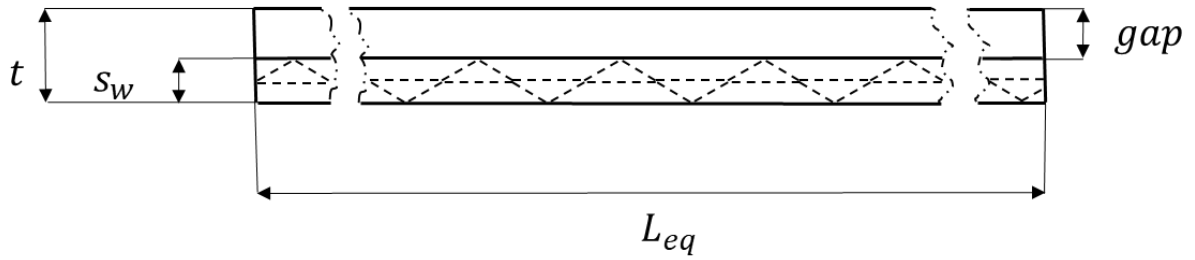


Figure 46 Scheme of the equivalent frontal section of the heat exchanger.

The length of this rectangle L_{eq} is calculated using the following formulas:

$$CS = \frac{\pi}{4}(D_e^2 - D_i^2) \quad (4.1)$$

$$t = s_w + gap \quad (4.2)$$

$$L_{eq} = \frac{CS}{t} \quad (4.3)$$

Where CS is the cross section, s_w is the thickness of the plate and t is the sum of this one and the gap.

In order to calculate the hydraulic diameter of the two fluid more geometrical features have to be calculated.

The hydraulic diameter is defined as:

$$D_h = \frac{4 \cdot A}{P} \quad (4.4)$$

Where A and P are respectively the wetted surface and perimeter.

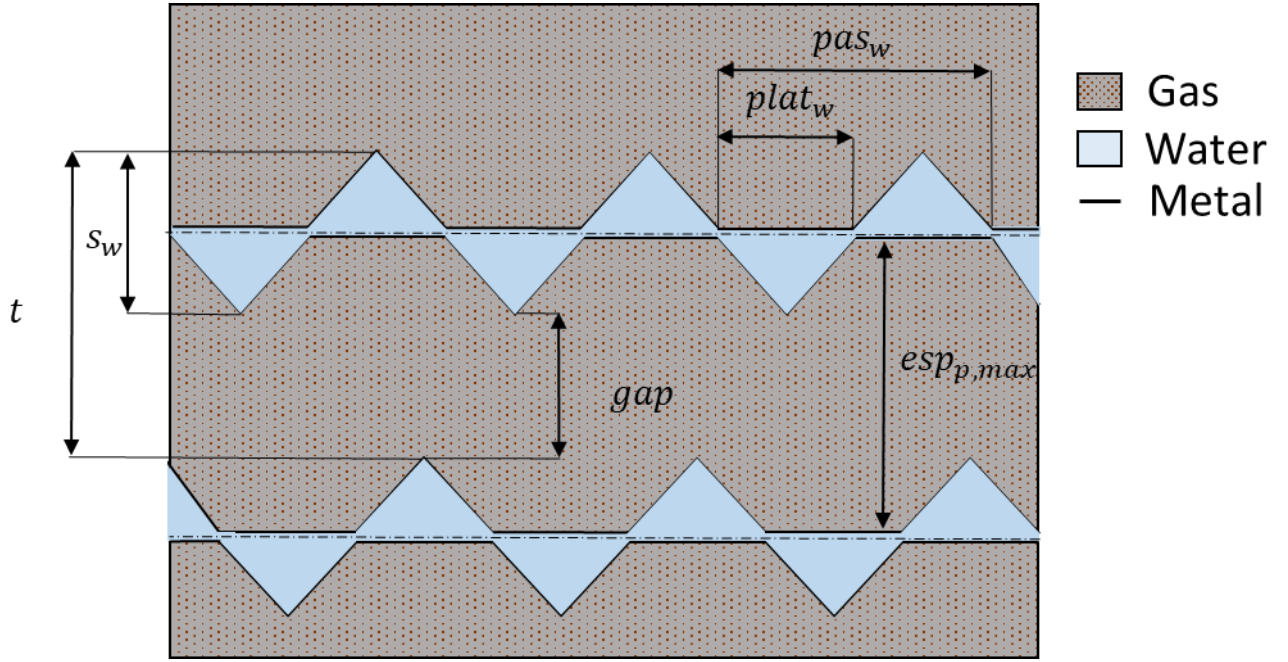


Figure 47 Scheme of the cross section of the HEX with the main geometrical dimensions.

Concerning the gas, the wetted area and perimeter are:

$$A_{gas,wetted} = esp_{p,gas} \cdot L_{eq} \quad (4.5)$$

$$P_{gas,wetted} = 2 \cdot (L_{eq} \cdot \Phi + esp_{p,gas}) \quad (4.6)$$

So from eq. 1:

$$D_{h,gas} = \frac{2 \cdot esp_{p,gas} \cdot L_{eq}}{L_{eq} \cdot \Phi + esp_{p,gas}} \quad (4.7)$$

Where Φ is the elongation factor, i.e. the ratio of the developed length to the protracted length, in this case equal to 1.35; and $esp_{p,gas}$ is the measure of the space where the gas flow and that is calculated by these formulas:

$$esp_{p,max} = gap + s_w - 2 \cdot s_m \quad (4.8)$$

$$esp_{p,gas} = esp_{p,max} - 2 \cdot DELTA \quad (4.9)$$

Where s_m is the thickness of the metal equal to 0.3 mm and $DELTA$ the surface roughness of the plate equal to 0.252 mm.

For the water side the wetted area and perimeter are:

$$A_{water,wetted} = 2 \cdot \frac{s_w}{2} \cdot \frac{pas_w - plat_w}{2} \quad (4.10)$$

$$P_{water,wetted} = 2 \cdot \Phi \cdot pas_w \quad (4.11)$$

So the hydraulic diameter is:

$$D_{h,w} = \frac{s_w \cdot (pas_w - plat_w)}{\Phi \cdot pas_w} \quad (4.12)$$

The cross section of the fluids is calculated as follow:

$$CS_{gas} = L \cdot esp_{p.gas} \quad (4.13)$$

$$CS_{water} = L \cdot s_w \cdot c_{\Delta} \quad (4.14)$$

It has to be noticed that the cross section for the water includes a factor c_{Δ} that stands for the ratio of the cross section of the triangles by the total cross section of the aluminium plate.

$$c_{\Delta} = \frac{CS_{\Delta}}{CS_{plate}} = 0.31 \quad (4.15)$$

As suggested by the ACTE company a factor of 0.9 is multiplied by the length of the plate to take into account that for what concerns the heat exchange, a part of the plate is useless since the flow is not completely developed.

$$L_P = 0.9 \cdot L_{HEX} \quad (4.16)$$

Finally it is possible to calculate A_{HEX} , i.e. the exchange surface of the heat exchanger:

$$A_{HEX} = 2 \cdot L_{eq} \cdot L_P \cdot \Phi \quad (4.17)$$

Finally, in Table 4 the main geometric parameters of the heat exchanger are listed.

Table 4 Geometry of the plate heat exchanger

Test section	Parameter	Symbol	Value
GAP heat exchanger	Mean Chevron angle	β	52.2°
	Corrugation pitch	pa_{sw}	4.72 mm
	Flat plat width	pl_{at_w}	1.33 mm
	Enlargement factor	Φ	1.36
	Gas hydraulic diameter	$D_{h_{gas}}$	7.1 mm
	Water hydraulic diameter	$D_{h_{water}}$	1.6 mm
	Gas cross sectional area	CS_{gas}	0.1163 m ²
	Water cross sectional area	CS_{water}	0.0221 m ²
	Heat transfer area	A_{HEX}	17.4281 m ²
	Length plate	L_{HEX}	302 mm
	Thickness of the plate	sw	3 mm
	Thickness of the gas passage	gap	3 mm

4.3 Heat transfer model

4.3.1 Introduction

In order to predict the thermal performances of the heat exchanger a model has been calibrated.

The model is a counter current semi-empirical model. The heat exchanger is divided into 1 or 3 zones depending if the cold fluid (water) is in liquid phase or in vapour phase at the outlet of the heat exchanger.

It is considered semi-empirical since it needs experimental results to calibrate some parameters.

The inputs are: the inlet temperatures, pressures and mass flow rate of both the cold and the hot fluid. It is also necessary the knowledge of the total heat transfer area, found in section 4.1, and of the heat transfer correlations of the two fluids.

The iterative parameter is the thermal power exchanged. The solution is in the range $(0, \dot{Q}_{max})$. The upper bound of this interval is the first guess of the iterative process and it is calculated through a methodology detailed in the section 4.2.2.

Once the heat transfer rate is known, the heat exchanger is divided into cells, and knowing the heat transfer correlation the fraction of the total heat exchange surface for each cell is calculated. The sum of the surface of each zone is then compared with the actual one.

The error on the exchange surface is then used to iterate on the total thermal power until a certain precision on the error is reached.

The model is based on the solution approach schematized with the flow chart in Figure 48.

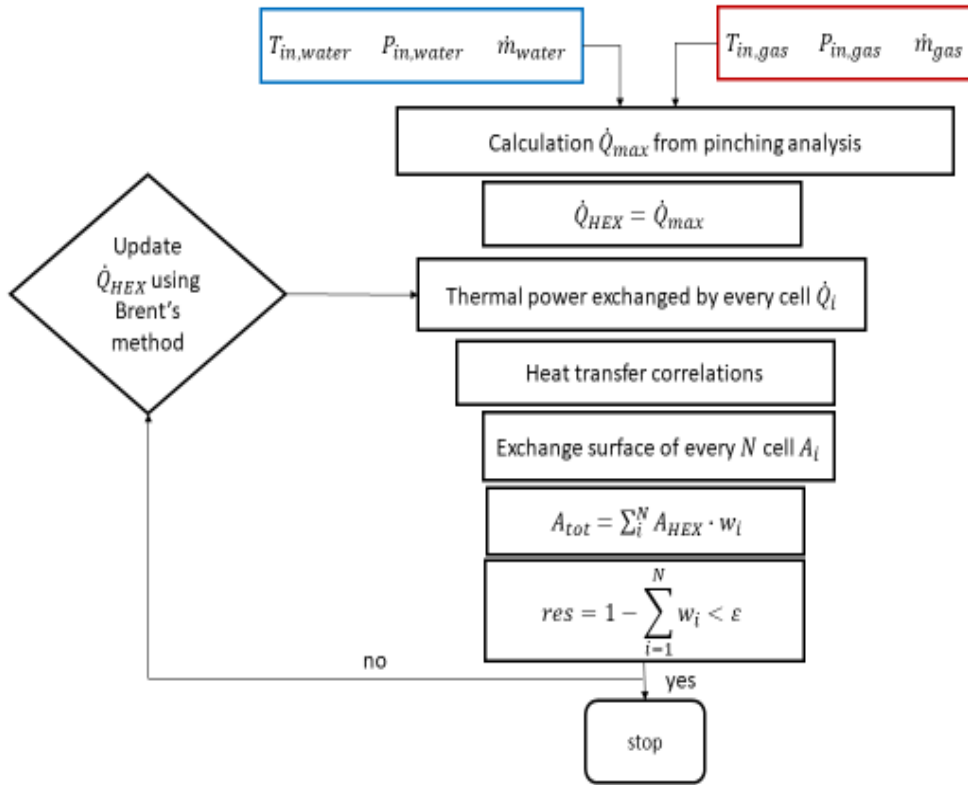


Figure 48 Flow chart representation of the algorithm

The output of the model are the numerical heat transfer rate \dot{Q}_{num} . This value is compared with the experimental heat transfer rate \dot{Q}_{exp} in order to calibrate the three parameters a, b, c used to calculate the Nusslet number of the gas in the heat transfer correlation written as:

$$Nu_{gas} = a \cdot Re^b \cdot Pr^c \quad (4.18)$$

Where Re and Pr are the Reynolds and the Prandtl number.

These three parameters have been found minimizing an error objective defined as the root mean square error of the numerical thermal power against the experimental one:

$$err_{\dot{Q}} = \frac{1}{\dot{Q}_{max} - \dot{Q}_{min}} \cdot \sqrt{\frac{\sum_{i=1}^N (\dot{Q}_{exp,i} - \dot{Q}_{num,i})^2}{N}} \quad (4.19)$$

Concerning the heat transfer correlation for the Nusselt number of the water two correlations, one for the single phase and another for the two phase have been taken from literature (Section 4.3.3).

The model is characterized by a solution approach based on [10], that will be detailed in the section 4.3.2.

4.3.2 Methodology: Maximum heat transfer rate and Cells division and analysis

The steps of the solution approach are three:

1. Calculation of the maximum possible heat transfer rate knowing the inlet condition of the two fluids, i.e. the inlet temperatures, the mass flow rate and the pressures, assuming only the external pinching (in Figure 49(a)).
2. Decrease the heat transfer rate taking into account the eventually present phase change of the water, and avoid impossible pinching configuration inside the heat exchanger (in Figure 49(b)).
3. Find through an iterative process the actual heat transfer using a bounded numerical solver that takes into account the physical bounds for the heat transfer rate(in Figure 49(c)).

Once the total heat transfer rate is known, it is possible to calculate the enthalpies of the two fluids at the inlet and at the outlet of the heat exchanger, being able to divide the heat exchanger in cells, where the fluids are in liquid, vapour or two-phase condition.

The bound from a cell to another is determined by the change of the thermodynamic state of one of the two fluids.

The detailed analysis required for each part of this solution approach will be covered in the following sections.

4.3.2.1 External pinching

From the second law of thermodynamic it is known that heat could be transferred only from a higher temperature source to a lower temperature one.

This law imposes a temperature limit that could be reached by the fluid at the outlet of the heat exchanger. At the outlet the hot fluid could be at a temperature not lower than the one of the cold fluid at the inlet, and the temperature of the cold fluid at the outlet could be not greater than the temperature of the hot fluid at the inlet.

These limits could be expressed by the equations:

$$T_{h,out} \geq T_{c,in} \quad (4.20)$$

$$T_{c,out} \leq T_{h,in} \quad (4.21)$$

Then it is possible to calculate the maximum heat transfer rate for the two fluids.

For the hot fluid:

$$\dot{Q}_{h,max} = \dot{m}_h \cdot (h_{h,in} - h_{h,out}) \quad (4.22)$$

Where $h_{h,out}$ is calculated at the inlet pressure of the hot fluid and at the inlet temperature of the cold fluid.

For the cold fluid:

$$\dot{Q}_{c,max} = \dot{m}_c \cdot (h_{c,out} - h_{c,in}) \quad (4.23)$$

Where $h_{c,out}$ is calculate at the inlet pressure of the cold fluid and at the inlet temperature of the hot fluid.

The maximum heat transfer rate by the external pinching analysis is given by:

$$\dot{Q}_{max,ext} = \min(\dot{Q}_{h,max}, \dot{Q}_{c,max}) \quad (4.24)$$

4.3.2.2 Internal pinching

The external pinch analysis does not take into account the temperatures profiles of the two fluid inside the heat exchanger.

In the case there is no phase change the equation (4) represent the maximum possible heat transfer rate.

On the contrary, in case of phase change inside the heat exchanger there is the possibility of a crossing temperature profiles of the two fluids, as shown in Figure 49(a).

This situation could lead to a physically impossible case where the hot fluid is colder than the cold one. In order to avoid this problem, the maximum possible heat transfer rate should be reduced.

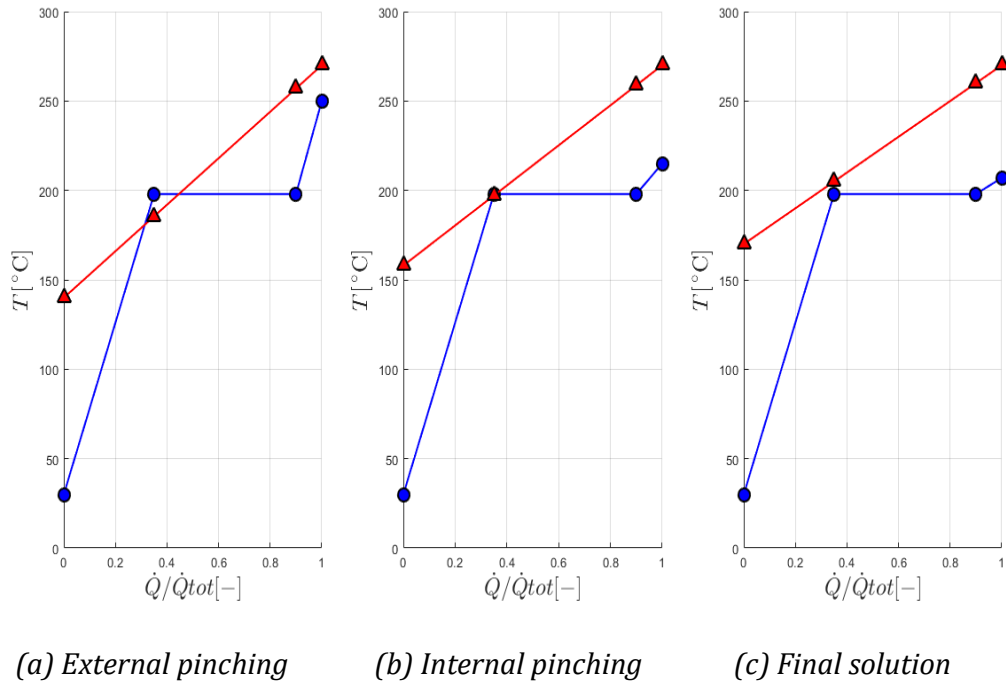


Figure 49 Schematic representation of the temperature profile of the two fluids inside the heat exchanger

First of all, knowing the $\dot{Q}_{max,ext}$ from the previous step, the heat exchanger is divided into three cells, where the enthalpies at the bound of each one is known doing a simple thermal balance.

At every cell boundary the temperature profile is evaluated. If in one point there is a crossing profile, an internal pinch point has been found. In this case the maximum heat transfer rate is reduced, carrying out a new cell division with the new maximum heat transfer rate predicted.

In Figure 49(a) it is shown a case where the external pinching analysis leads to a temperature of the hot fluid lower than the cold fluid, in the two-phase cell.

The objective is to calculate a new heat transfer rate that leads to an equal temperature of the two fluids at the pinch point, as in Figure 49(b).

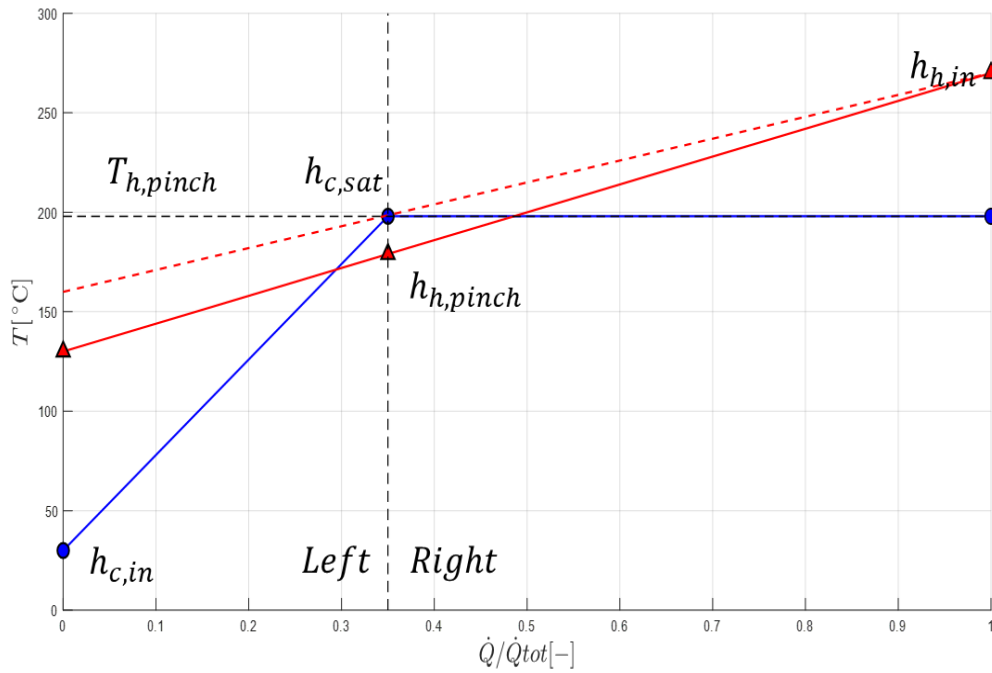


Figure 50 Schematic representation of an internal pinch point

In order to satisfy this condition, the scheme is divided in two parts, as represented in Figure 50 where the dashed red line represent the temperature profile of the hot fluid to satisfy the pinch point equal to zero condition previously stated.

In the left part, knowing as a model input the inlet enthalpy of the cold fluid $h_{c,in}$, and knowing its saturation temperature T_{sat} from its inlet pressure $P_{c,in}$, it is possible to calculate the thermal power transferred in the left part as:

$$\dot{Q}_{left} = \dot{m}_c \cdot (h_{sat} - h_{c,in}) \quad (4.25)$$

In the right part, in order to satisfy the condition of an equal temperature of the two fluids at the pinch point, considering as know the inlet condition of the hot fluid, as it is for the cold fluid, it is possible to calculate the thermal power transferred in the right part as:

$$\dot{Q}_{right} = \dot{m}_h \cdot (h_{h,pinch} - h_{h,in}) \quad (4.26)$$

Where:

$$h_{h,pinch} = h(T_{pinch}, P_{h,in}) \quad (4.27)$$

Finally, the new guess for the maximum possible heat transfer rate is the summation of the two thermal powers:

$$\dot{Q}_{max,int} = \dot{Q}_{left} + \dot{Q}_{right} \quad (4.28)$$

This leads to the final solution in Figure 49(c).

4.3.2.3 Cells division and analysis

When the $\dot{Q}_{max,int}$ is calculated the heat exchanger is divided into a number N of j cells, that could be 1 if the cold fluid stays in liquid phase till the outlet or 3 if it is in over-heated vapour conditions. Every cell has two boundaries, for a total number of $N+1$, indicated with the subscript i .

The enthalpies at the boundaries are calculated from the conservation of power inside the cell.

The thermal balance at each cell can be written as:

$$\dot{m}_h \cdot (h_{h,i+1} - h_{h,i}) = \dot{m}_c \cdot (h_{c,i+1} - h_{c,i}) \quad (4.29)$$

From this equation it is possible to calculate the enthalpies, and so the temperature of the two fluids at each boundary.

Once the cell division of the heat exchanger is carried out, it is possible to calculate the fraction of the total exchange surface that every cell need.

It is known that the heat transfer for each cell \dot{Q}_j is the product of the exchange area A_j , the overall heat transfer coefficient U_j and the mean logarithmic temperature difference $LMTD_j$ [11] :

$$\dot{Q}_j = A_j \cdot U_j \cdot LMTD_j \quad (4.30)$$

The logarithmic mean temperature difference is equal to [11]:

$$LMTD_j = \frac{\Delta T_{1,j} - \Delta T_{2,j}}{\ln\left(\frac{\Delta T_{1,j}}{\Delta T_{2,j}}\right)} \quad (4.31)$$

Where $\Delta T_{1,j}$ and $\Delta T_{2,j}$ are the difference of the temperature of the two fluid respectively at the inlet and at the outlet of the cell.

Knowing the thickness of the metal s_m , its thermal conductivity k_m , and the heat transfer coefficient calculated in 4.3.3 section for the water and from eq. (4.18) for the gas, the overall heat transfer coefficient is given by:

$$U_j = \left(\frac{1}{h_{water}} + \frac{s_m}{k_m} + \frac{1}{h_{gas}} \right)^{-1} \quad (4.32)$$

In this way the last step is to calculate the exchange surface needed by the j cell:

$$A_j = \frac{\dot{Q}_j}{LMTD_j \cdot U_j} \quad (4.33)$$

And then its fraction w_j , defined as the ratio between the area needed to the total exchange surface of the heat exchanger A_{HEX} , calculated in section 4.1:

$$w_j = \frac{A_j}{A_{HEX}} \quad (4.34)$$

The evaluation of the total heat transfer rate is then calculated through an iterative process in the range of $(0, \dot{Q}_{max,int})$ driving to zero the residual function defined as:

$$res(\dot{Q}) = 1 - \sum_{j=1}^N w_j \quad (4.35)$$

In other words, the cell boundaries are recalculated till the sum of the fractions of the total heat transfer surface is equal to 1.

The Brent's method [12] has been chosen instead of the Newton's method as the numerical solver for this problem, since "[...] Newton's method cannot be easily applied to the residual function due to the generally large difference in slope of the residual function at $\dot{Q} = 0$ and $\dot{Q} = \dot{Q}_{max}$. [...]" [10].

4.3.3 Water heat transfer correlations

Concerning the Nusselt correlations for the water, in [13] a survey of correlations is listed for the single-phase in brazed plate heat exchanger.

In this case the Wanniarachchi et al. correlation [14] was used since it is proven in a wide range of Reynolds number that include the one tested in this work, which values are presented in Table 3.

The correlation for the Nusselt in single phase condition is:

$$Nu = (Nu_{lam}^3 + Nu_{turb}^3)^{\frac{1}{3}} \cdot Pr^{\frac{1}{3}} \cdot (\mu/\mu_w)^{0.17} \quad (4.36)$$

$$Nu_{lam} = 3.65 \cdot \beta^{-0.455} \cdot \Phi^{0.661} \cdot Re^{0.339} \quad (4.37)$$

$$Nu_{turb} = 12.6 \cdot \beta^{-1.142} \cdot \Phi^{1-m} \cdot Re^m \quad (4.38)$$

$$m = 0.646 + 0.0011 \cdot \beta \quad (4.39)$$

Where μ and μ_w are respectively the dynamic viscosity of the fluid at the bulk temperature and at the wall temperature.

Since the chevron angle β change from 45° to 60° along the plate, the average of this two values is taken in consideration.

For the two phase the Han et al. [15] correlation is considered:

$$Nu = Ge_1 \cdot Re_{c,eq}^{Ge_2} \cdot Bo^{0.3} Pr_{c,l}^{0.4} \quad (4.40)$$

$$Ge_1 = 2.81 \cdot \left(\frac{S_w}{D_{h,water}} \right)^{-0.041} \cdot \beta^{-2.83} \quad (4.41)$$

$$Ge_2 = 0.746 \cdot \left(\frac{S_w}{D_{h,water}} \right)^{-0.082} \cdot \beta^{0.61} \quad (4.42)$$

$$Gc_{eq} = Gc \cdot \left[(1 - x_c) + x_c \cdot \left(\frac{\rho_l}{\rho_v} \right)^{0.5} \right] \quad (4.43)$$

$$Gc = \frac{\dot{m}_w}{CS_w} \quad (4.44)$$

$$Bo = \frac{q}{Gc_{eq} \cdot i_{fg,c}} \quad (4.45)$$

4.3.4 Comparison experimental results with numerical

Based on the methodology presented in section 4.3.23, the three parameters a , b and c that express the gas heat transfer correlation, have been calibrated in order to minimize the error on the prediction of the thermal power exchanged.

The values of this three parameters are: $a = 0.0265$, $b = 0.781$ and $c = 0.4$.

In the following parity plots the agreement between the experimental thermal power exchanged in the heat exchanger and the one predicted by the model is shown for both the Heat to heat and the Evaporator mode (Figure 51 and Figure 52).

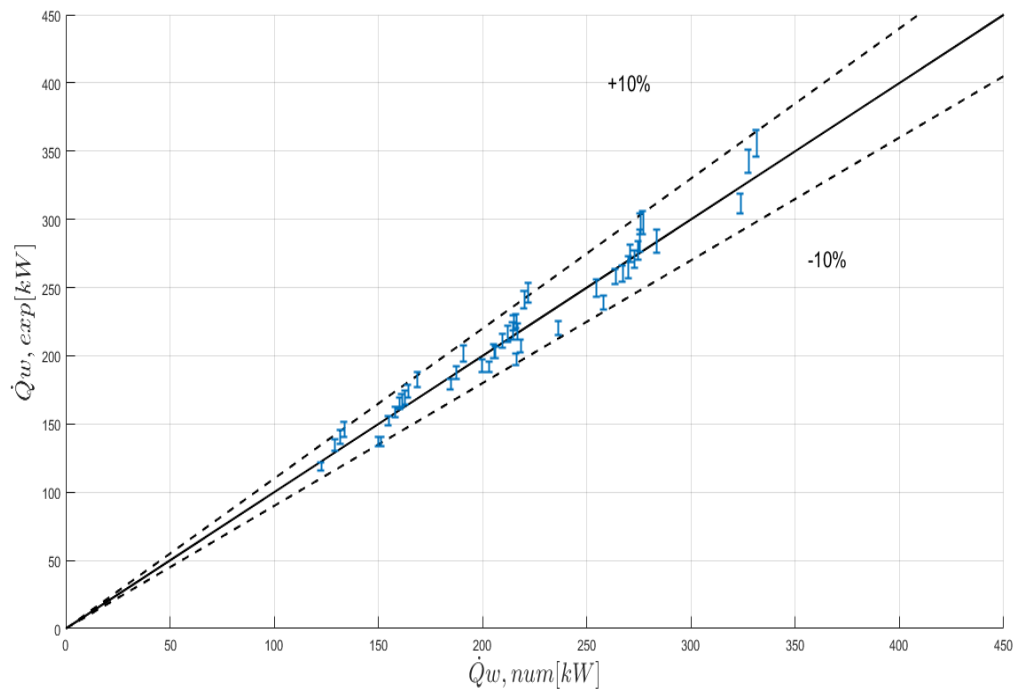


Figure 51 Heat to heat mode: Parity plot of the heat transfer rate (simulation results vs. experimental data).

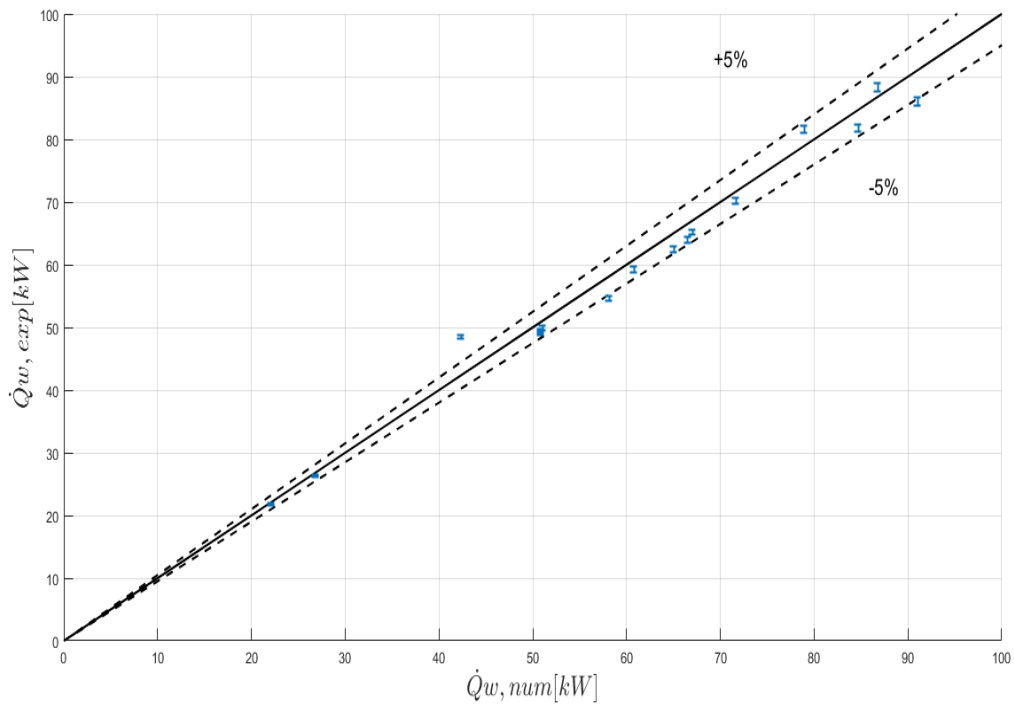


Figure 52 Evaporator mode: Parity plot of the heat transfer rate (simulation results vs. experimental data).

The model predicts the data in Heat to heat mode with an absolute mean error of 4.2% with all the points that fit in a bandwidth of 10%.

For the Evaporator mode the data are predicted with an absolute mean error of 3.2% with the 95% of the points that fit in a bandwidth of 5%.

In conclusion, the calibrated model can be trusted because of the decent error on the simulation of performance.

4.4 Pressure drop model

4.4.1 Methodology

Concerning the prediction method of the pressure drop a model has been implemented, taking into account the concentrated and the distributed pressure drops that the fluids experience flowing into the heat exchanger.

At the inlet of the heat exchanger the gas has a sudden contraction due to the restriction of its passage section caused by the presence of the three water collectors and then a sudden expansion due to the enlargement of the tube section where it is flowing in.

At the outlet it is the contrary, i.e. a sudden contraction and then a sudden expansion in the duct.

The gas sees its passage section going from the total cross section of the heat exchanger CS , to the total cross section minus the one of the collectors CS_{at} , then to its cross section in the heat exchanger CS_{gas} , and then obviously again to CS_{at} and finally to CS .

The total pressure drop experienced by the gas along the heat exchanger can be written as:

$$\Delta P_{tot,gas} = \Delta P_{contr,1} + \Delta P_{exp,1} + \Delta P_{distributed} + \Delta P_{contr,2} + \Delta P_{exp,2} \quad (4.46)$$

On the water side the pressure drop was modelled considering the expansion of the fluid from the collectors to the space of the plate where the water flows in, the frictional distributed charge losses along the plates, and the contraction of the fluid when this one is collected by the three collectors at the border of the plate:

$$\Delta P_{tot,water} = \Delta P_{expansion} + \Delta P_{distributed} + \Delta P_{contraction} \quad (4.47)$$

4.4.1.1 Local pressure drop: Expansion

The general equation to calculate a concentrated pressure drop is [11]:

$$\Delta P = K \cdot \rho \cdot \frac{v^2}{2} \quad (4.48)$$

where v [m/s] is the velocity of the fluid in the conduit, ρ [kg/m³] is its density, and K is a factor that depends on the geometry of the restriction, enlargement, or deviation of the section of the duct, and on its thermo-fluid dynamic conditions, often represented by the Reynolds number.

As suggest in [16] in case of a sudden expansion of the flow from a section S_0 to a larger one S_1 , if the fluid is in turbulent condition ($Re > 2300$) the coefficient K is defined as:

$$K_{expansion} = 1 - \frac{S_0}{S_1} \quad (4.49)$$

Since the gas it's always characterized by a Reynolds number greater then 2300, this equation has been used,

The first expansion coefficient for the gas is:

$$K_{expansion,1} = 1 - \frac{CS_{at}}{CS_{gas}} \quad (4.50)$$

Where CS_{at} is the total cross section of the gas minus the one occupied by the aluminium plate and the one occupied by the collectors:

$$CS_{at} = (CS - L_{eq} \cdot s_w) \cdot (1 - \gamma) \quad (4.51)$$

γ represent the ratio of the section of the collectors to the total cross section of the heat exchanger defined as:

$$\gamma = N_{collectors} \cdot \frac{\theta}{360} \quad (4.52)$$

Where $N_{collectors}$ is the number of collectors at the inlet(or outlet) equal to 3, and θ is the aperture angle of a collector equal to 20° .

The second expansion coefficient for the gas is:

$$K_{expansion,2} = 1 - \frac{CS_{at}}{CS} \quad (4.53)$$

Since the water is in all the test is in the laminar region, the expression for the local resistance coefficient has been determined from the following equation taken from curves in [8]:

- $500 \leq Re \leq 2300$

$$K = -8.445 - 26.163 * (1 - \sigma)^2 - 5.38086 * (1 - \sigma)^4 + \log_{10}(Re) * (6.007 + 18.5372 * (1 - \sigma)^2 + 3.9978 * (1 - \sigma)^4) + \log_{10}(Re)^2 * (-1.02318 - 3.0916 * (1 - \sigma)^2 - 0.680943 * (1 - \sigma^4)) \quad (4.54)$$

- $10 \leq Re < 500$

$$\begin{aligned}
K = & 3.62536 + 10.744 * (1 - \sigma)^2 - 4.41041 * (1 - \sigma^4 + 1/\log_{10}(Re) * (-18.13 \\
& - 56.77855 * (1 - \sigma)^2 + 33.40344 * (1 - \sigma)^4) + 1/\log_{10}(Re)^2 \\
& * (30.8558 + 99.9542 * (1 - \sigma)^2 - 62.78 * (1 - \sigma)^4) + 1/\log_{10}(Re)^3 \\
& * (-13.217 - 53.9555 * (1 - \sigma)^2 + 33.8053 * (1 - \sigma)^4) \quad (4.55)
\end{aligned}$$

- $Re < 10$

$$K = \frac{30}{Re} \quad (4.56)$$

Where the coefficient C is defined as:

$$\sigma = 1 - \frac{CS_{collectors}}{CS_{water}} \quad (4.57)$$

$CS_{collectors}$ is the cross section of the collectors, equal to:

$$CS_{collectors} = CS_{water} \cdot \gamma \quad (4.58)$$

4.4.1.2 Local pressure drop: Contraction

As stated in [16] the local resistance coefficient in case of a sudden contraction of the flow that goes from a conduit of cross section S_1 to one with a smaller cross section S_0 depends on the dynamic conditions of the fluid.

In case the flow is in the laminar region ($Re < 2300$), the local resistance coefficient is equal to:

$$K_{contraction,lam} = \frac{30}{Re} \quad (4.59)$$

In case the flow is in the transition/turbulent region ($Re > 2300$):

$$K_{contraction,turb} = A \cdot B \cdot \left(1 - \frac{S_0}{S_1}\right) \quad (4.60)$$

Where A is calculated as:

$$A = \sum_{i=0}^7 a_i \cdot (\log Re)^i \quad (4.61)$$

Where a is a vector of elements equal to:

$$a_0 = -25.12458; \quad a_1 = 118.5076; \quad a_2 = -170.4147; \quad a_3 = 118.4969;$$

$$a_4 = -44.42141; \quad a_5 = 9.09524; \quad a_6 = -0.9244027; \quad a_7 = 0.034208$$

The coefficient B is calculated with the following equation:

$$B = \sum_{i=0}^2 \left\{ \left[\sum_{j=0}^2 b_{i,j} \cdot \left(\frac{S_0}{S_1}\right)^j \right] \cdot (\log Re)^i \right\} \quad (4.62)$$

Where $b_{i,j}$ is the element of a matrix of i rows and j columns that differs in the case the flow is laminar or turbulent (Table 4).

Table 5 Values of b_{ij} [16]

	10 ≤ Re ≤ 2000			2000 ≤ Re ≤ 1000		
i/j	0	1	2	0	1	2
0	1.07	1.22	2.9333	0.5443	-17.298	-40.715
1	0.05	-0.51668	0.8333	-0.06518	8.7616	22.782
2	0	0	0	0.05239	-1.1093	-3.1509

4.4.1.3 Distributed pressure drop

In general, the distributed pressure drop of a fluid along a conduit is equal to:

$$\Delta P_{distributed} = f \cdot \frac{L}{D_h} \cdot \rho \cdot \frac{v^2}{2} \quad (4.63)$$

Where f is the friction factor and L is the length of the conduit.

The distributed pressure drop for the water is equal to:

$$\Delta P_{water,distributed} = C_w \cdot f_{water} \cdot \frac{L_w}{D_{h,water}} \cdot \rho \cdot \frac{v^2}{2} \quad (4.64)$$

Where C is a corrective factor calculated in order to minimize the error between the experimental and the simulated pressure drop:

$$err_{\Delta P_w} = \frac{1}{\Delta P_{w,max} - \Delta P_{w,min}} \cdot \sqrt{\frac{\sum_{i=1}^N (\Delta P_{w,exp,i} - \Delta P_{w,num,i})^2}{N}} \quad (4.65)$$

The friction factor f_{water} is calculated with the Wanniarachchi et al. [9] correlation:

$$f_{water} = [f_l^3 + f_t^3]^{1/3} \quad (4.66)$$

The subscripts l and t of the two friction factors stay for laminar and turbulent, and they are equal to:

$$f_l = 1744 \cdot [\beta]^{-1.026} \cdot [\phi]^2 \cdot Re^{-1} \quad (4.67)$$

$$f_t = 46.6 \cdot [\beta]^{-1.08} \cdot [\phi]^{1+p} \cdot Re^{-p} \quad (4.68)$$

Where p is a constant depending only on the chevron angle β :

$$p = 0.00423 \cdot [\beta] + 0.0000223 \cdot [\beta]^2 \quad (4.69)$$

Concerning the distributed pressure drop on the gas side a methodology found in [8] for a circular cross section conduit has been used.

Since the gas does not flow in a cylinder, a coefficient C_{AR} , due to the different aspect ratio “seen” by the gas, has been fitted in the following equation:

$$\Delta P_{gas,distributed} = C_g \cdot f_{gas} \cdot \frac{L_g}{D_{h,gas}} \cdot \frac{v^2}{2} \quad (4.70)$$

The coefficient C_g has been found minimizing the error between the experimental gas pressure drop and the predicted one:

$$err_{\Delta P_{gas}} = \frac{1}{\Delta P_{gas,max} - \Delta P_{gas,min}} \cdot \sqrt{\frac{\sum_{i=1}^N (\Delta P_{gas,exp,i} - \Delta P_{gas,num,i})^2}{N}} \quad (4.71)$$

For a circular duct the friction factor is equal to:

$$f_{gas} = \frac{1}{[a + b \cdot \log(Re \cdot \sqrt{f_{gas}}) + c \cdot \log \bar{\Delta}]^2} \quad (4.72)$$

Where $\bar{\Delta}$ is equal to the ratio of the mean roughness to the hydraulic diameter of the gas:

$$\bar{\Delta} = \frac{\Delta}{D_{h,gas}} \quad (4.73)$$

The values of the coefficient a, b and c depends on the value of χ equal to:

$$\chi = Re \cdot \bar{\Delta} \cdot \sqrt{f_{gas}} \quad (4.74)$$

$$10 \leq \chi < 20$$

$$a = 0.068; b = 1.13 ; c = -0.87 ;$$

$$20 \leq \chi < 40$$

$$a = 1.538; b = 0 ; c = -2 ;$$

$$40 \leq \chi \leq 191.2$$

$$a = 2.471; b = -0.588 ; c = -2.588 ;$$

$$\chi > 191.2$$

$$a = 1.138; b = 0 ; c = -2 ;$$

In order to calculate the friction factor an iterative process has been implemented since it is given in a non-linear system of equations.

4.4.2 Comparison experimental results with numerical

In the following parity plots the agreement between the experimental pressure drop along the heat exchanger and the one predicted by the models is shown for both the gas (Figure 53) and the water (Figure 54).

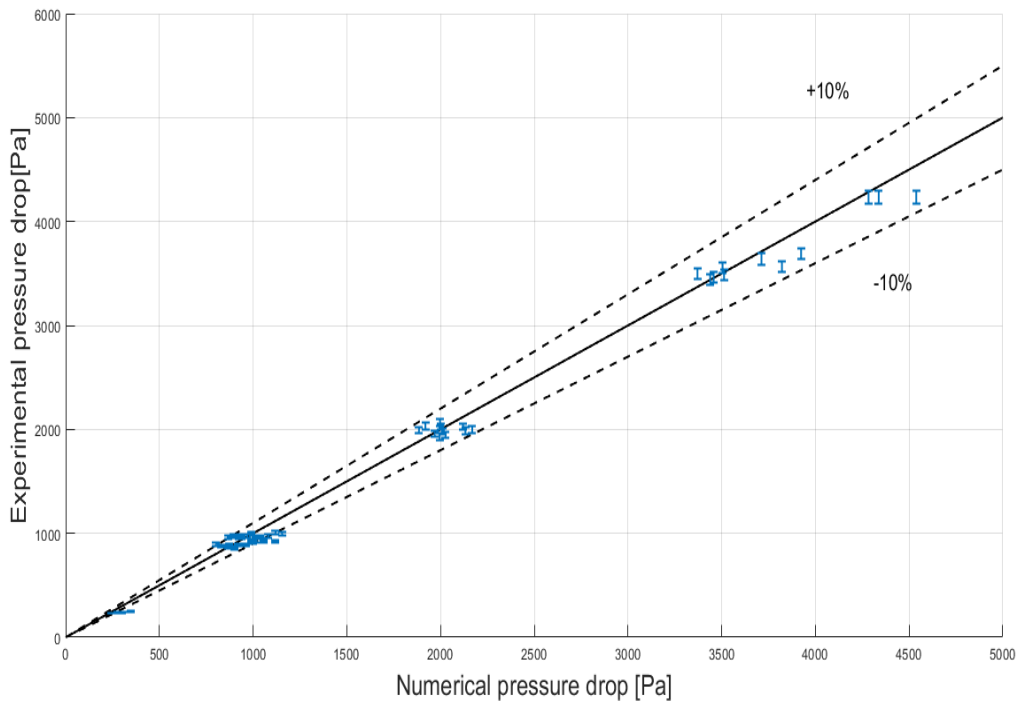


Figure 53 Heat to heat and Evaporator mode: Parity plot of the gas pressure drop(simulation results vs. experimental data).

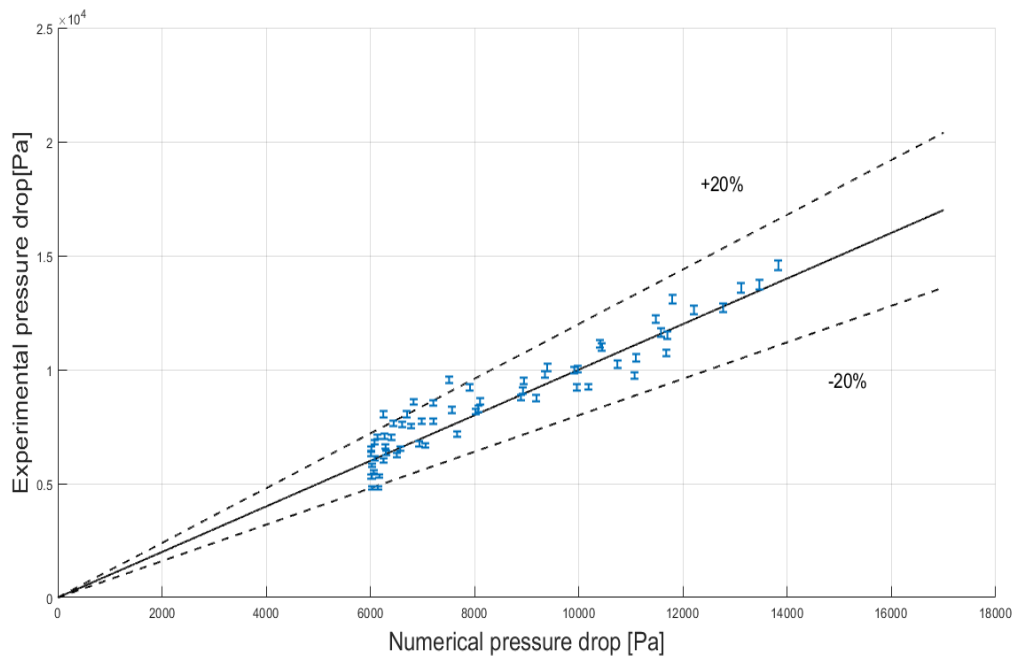


Figure 54 Heat to heat mode: Parity plot of the water pressure drop(simulation results vs. experimental data).

The corrective factor of the distributed pressure drop correlation found from the iterative process are $C_w = 0.751$ and $C_g = 1.587$.

The model predicts the data for the gas pressure drop with an absolute mean error of 6.4% whit all the points that fit in a bandwidth of 10%.

For the Evaporator mode the data are predicted with an absolute mean error of 14.7% whit the 90% of the points that fit in a bandwidth of 20%.

In conclusion, the pressure drop model gives satisfying results due to the relative low error between the experimental and the simulated points, especially for the gas where the pressure drop are considered of a crucial importance for this application as discussed in the introduction.

4.5 Conclusions

The numerical model, based on calibrated correlation, is able to predict the thermal power exchanged and the pressure drop of the two fluids in the heat exchanger with a good accuracy.

Thanks to this model it is possible to evaluate the performances of a Rankine Cycle, where the heat exchanger is the evaporator, in a large range of temperatures and mass flow rate of the exhaust gas.

5 Integration of the model in a Rankine Cycle

5.1 Introduction

In this chapter the model of the heat exchanger, discussed in the previous section, is integrated in a Rankine cycle model as the evaporator.

The objective of this section is to analyze the performances of the Rankine cycle in terms of electric power delivered at the expander and its global efficiency.

Firstly, the model of the cycle is introduced with all the assumption and the hypothesis used to calculate the thermal balances on each component.

Then a parametric analysis is performed on the model varying all the parameters that have an impact on the calculation of the power and efficiency of the cycle.

Finally, the main results are presented and discussed in the paragraph 5.4.

5.2 Steam Rankine Cycle Model

5.2.1 Introduction

The steam Rankine cycle model took as input the evaporation pressure P_{ev} , the condensation temperature of the water T_{cd} , the overheating OH, the sub-cooling SC, the gas mass flow rate \dot{m}_{gas} and the supply temperature of the gas $T_{su,gas}$.

The water mass flow rate \dot{m}_{water} is the iterative parameter of the model. Once the sub-cooling at the condenser and the condensing temperature of the cycle are imposed, the inlet conditions of the fluid at the evaporator are known.

Then imposing the over-heating and the evaporation pressure of the cycle, the state of the water at the outlet of the evaporator is also known. At this point, knowing the inlet temperature, pressure and mass flow rate of the heat source, the heat exchanger model presented in the previous chapter is exploited to calculate the water mass flow rate needed to reach the outlet enthalpy imposed.

The output of the model are the mass flow rate of the water \dot{m}_{water} , the electric power produced by the expander \dot{W}_{el} , the efficiency of the cycle (ϵ) and the thermal power at the condenser \dot{Q}_{cd} .

In Figure 55 the hydraulic scheme of the cycle is shown. The main points of the cycle, with the thermal and mechanical fluxes, are highlighted.

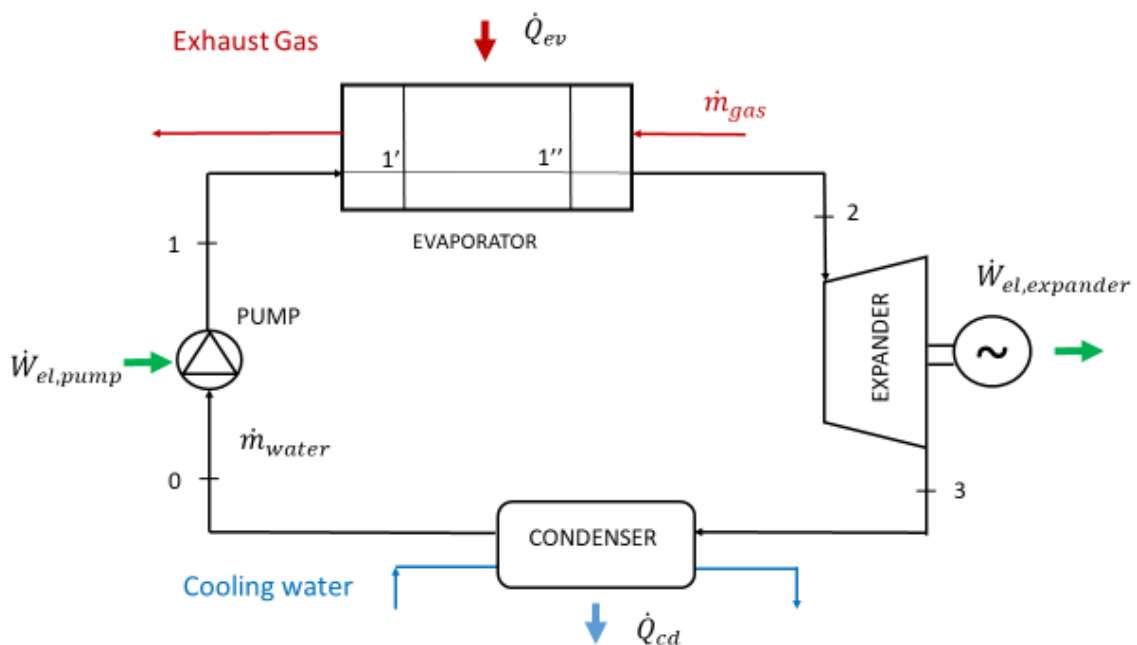


Figure 55 Hydraulic scheme of the Rankine Cycle

In Figure 56 the temperature-entropy diagram of the water is plotted. The red line represents the temperature profile of the exhaust gases, while the blue line is the temperature profile of the cooling water of the condenser. The point 0 and 1 are almost coincident on the T-s diagram as it can be noticed in Figure 56. Figure 56 Temperature-Entropy diagram of the Rankine Cycle Figure 56.

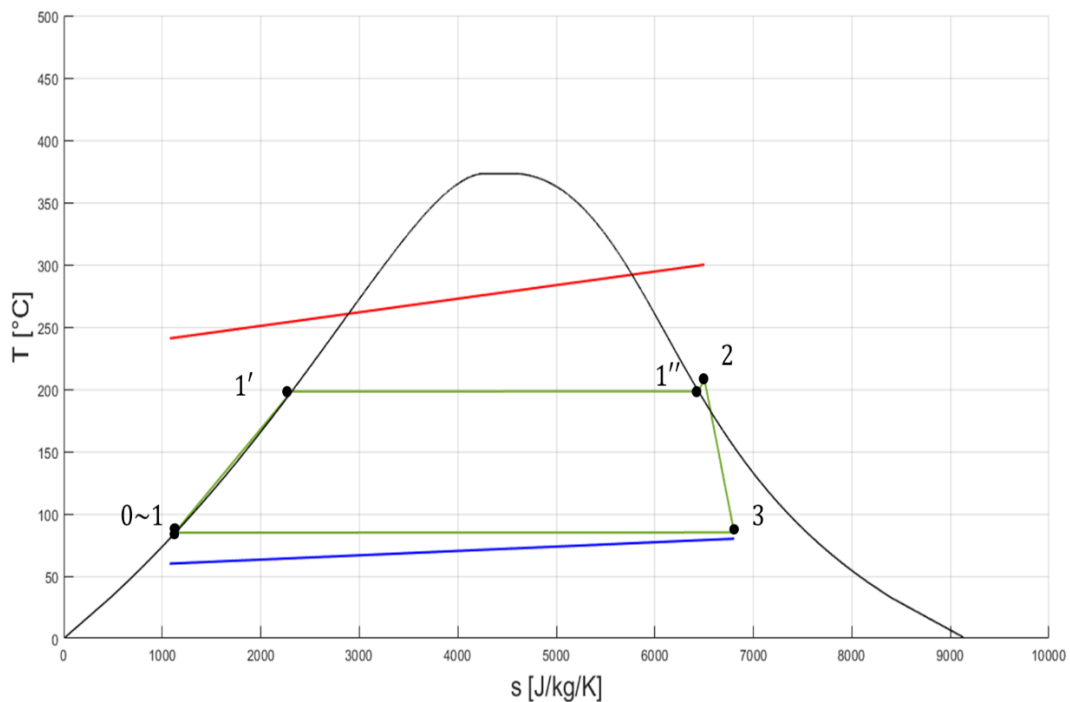


Figure 56 Temperature-Entropy diagram of the Rankine Cycle

In the following sections the thermal balance, the assumption and the hypothesis on each component of the cycle are detailed.

5.2.2 Pump

The Pump is assumed adiabatic, i.e. no heat transfer rate is exchanged from the machine to the ambient and vice versa, and characterized by a constant efficiency, and not depending on the working condition of the machine.

The inlet conditions of the pump (0) are calculated from the imposed condensing temperature and sub-cooling on the thermodynamic cycle.

The sub-cooling is considered constant and equal to 5 K.

The sub-cooling is defined as:

$$SC = T_{cd} - T_0 \quad (5.1)$$

From this equation, it is possible to calculate T_0 , i.e. the temperature of the water at the inlet of the pump. It is important to cool down the water in the condenser below the condensing pressure in order to avoid the creation of vapor inside the pump.

This could lead to the presence of cavitation into the machine causing irreversible technical problems.

The inlet pressure of the pump is calculated as:

$$P_0 = P(Q = 0, T = T_0, \text{water}) \quad (5.2)$$

The definition of efficiency for a pump is the ratio between the actual pump work and the electric power absorbed by the machine [1]:

$$\eta_{el,pump} = \frac{\dot{V}_{water} \cdot (P_{ex} - P_{su})}{W_{el,pump}} \quad (5.3)$$

Where the pressure at the outlet is equal to the evaporating pressure of the cycle P_{ev} , and the inlet pressure is the one at the point 0 of the cycle.

Considering a conversion efficiency of the electrical motor that drive the pump equal to 0.85, the electrical power needed is:

$$\dot{W}_{el,pump} = \frac{\dot{V}_{water} \cdot (P_{ex} - P_{su})}{\eta_{el,pump}} \quad (5.4)$$

5.2.3 Evaporator

The evaporator is assumed to have no thermal losses to the ambient, and negligible pressure drop on the water side.

These two assumption have been verified in the experimental results in the Chapter 3.

At constant evaporating and condensing pressure, higher is the over-heating higher is the cycle efficiency, but lower is the output power since the mass flow rate of the working fluid is lower.

Since increasing the over-heating gives relatively low improving on increasing the cycle efficiency, it is better to reduce it as much as possible in order to increase the power at the expander.

For these reasons, the overheating at a first approximation is considered constant and equal to 10 K.

The overheating is defined as:

$$OH = T_2 - T_{ev} \quad (5.5)$$

Where T_{ev} is the evaporation temperature of the water calculated imposing the evaporation pressure of the cycle:

$$T_{ev} = T(Q = 0; P = P_{ev, water})$$

Where Q is the quality of the fluid.

From eq. (5.5) the temperature of the fluid at the outlet of the evaporator can be calculated, and then its enthalpy:

$$h_2 = h(T = T_2, P = P_{ev, water})$$

Once the enthalpy of the water at the outlet of the evaporator is calculated, the water mass flow rate is iterated on the heat exchanger model presented in the chapter 2, until the difference between the enthalpy calculated h_2 and the one given by the model h_2' is smaller than a certain tolerance of 1%

From the iterative process, the water mass flow rate needed is calculated.

The thermal balance on the evaporator can be written as:

$$\dot{Q}_{gas} - \dot{Q}_{ev} - \dot{Q}_{loss} = 0 \quad (5.6)$$

Where, as explained before $\dot{Q}_{loss} \sim 0$.

So, the power received at the evaporator by the water is equal to:

$$\dot{Q}_{ev} = \dot{m}_{water} \cdot (h_2 - h_1) \quad (5.7)$$

5.2.4 Expander

The hypothesis on the expander are the same as the pump.

It is considered an adiabatic device, with a constant isentropic efficiency, that does not depend on the working conditions of the machine. The state of the fluid at the inlet, point 2 on the scheme, is known, since it is an input of the Rankine Cycle model.

To calculate the outlet state of the fluid, the definition of the isentropic efficiency for an expansion machine is exploited.

It is defined as the ratio between the actual expander work and the isentropic one, as in the following equation [16]:

$$\eta_{is,expander} = \frac{h_2 - h_3}{h_2 - h_{3,is}} \quad (5.8)$$

The entropy at the point 2 is:

$$s_2 = s(T = T_2, P = P_{ev}, water)$$

From the definition of isentropic efficiency, the point 3_{is} has the same entropy of 2. Then the enthalpy of the fluid in isentropic condition is:

$$h_{3,is} = h(s = s_2, P = P_{cd}, water)$$

From eq. 2 the actual enthalpy at the outlet of the expander h_3 is given:

$$h_3 = h_2 - \eta_{is,expander} \cdot (h_2 - h_{3,is}) \quad (5.9)$$

As it can be noticed in *Figure 56* the enthalpy of the water at the outlet of the expander “falls” inside the two-phase zone of the diagram. This is due to the relatively low overheating imposed equal to 10 K.

That means that in the last stages of the machine liquid is also present with the vapor.

Since these outlet thermodynamic conditions are considered problematic for a turbine, a volumetric expander, like a screw expander could represent a most suitable solution.

This is also due to the fact that in order to have only vapor at that stage would lead to a much lower water mass flow rate with a consequently decrease of the mechanical power produce by the machine.

It is then possible to evaluate the mechanical power produced by the expander from;

$$\dot{W}_{mech,expander} = \dot{m}_{water} \cdot (h_2 - h_3) \quad (5.10)$$

Assuming as conversion efficiency of the electric alternator $\eta_{el, expander}$ constant and equal to 0.85, the electric power produced is:

$$\dot{W}_{el,expander} = \eta_{el,expander} \cdot \dot{W}_{mech,expander} \quad (5.11)$$

5.2.5 Condenser

The condenser was modelled as a counter-flow heat exchanger. The thermal losses to the ambient and the pressure drop are considered negligible.

From the thermal balance on the expander the inlet enthalpy of the water h_3 is known, as the outlet enthalpy h_0 given as an input of the model.

Therefore, the thermal power released at the condenser in the Rankine Cycle is equal to:

$$\dot{Q}_{cd} = \dot{m}_{water} \cdot (h_3 - h_0) \quad (5.12)$$

The condenser is supposed to be cooled by tap water that experience a temperature difference along the condenser ΔT_{glide} equal to 10 K(glide).

The mass flow rate of the cooling water in the condenser is calculated as:

$$\dot{m}_{cw} = \frac{\dot{Q}_{cd}}{c_p \cdot \Delta T_{glide}} \quad (5.13)$$

Where c_p is the specific heat capacity of the water at a constant pressure.

Then it is possible to evaluate the global efficiency of the Rankine cycle as the ratio between the net electric power produced to the thermal power extracted at the evaporator:

$$\eta_{cycle} = \frac{\dot{W}_{el,expander} - \dot{W}_{el,pump}}{\dot{Q}_{ev}} \quad (5.14)$$

Finally, the balance of the plant, i.e. the sum of all the thermal and mechanical power entering and exiting the cycle, is verified to be equal to 0:

$$\dot{Q}_{ev} - \dot{Q}_{cd} - \dot{W}_{mech,expander} + \dot{W}_{mech,pump} = 0 \quad (5.15)$$

5.3 Parametric Analysis

In this paragraph a parametric analysis of the Rankine Cycle is performed varying the parameters that have an influence on the efficiency and on the electric power produced.

5.3.1 Efficiency of the Cycle

First of all, in order to understand better the factors that influence the cycle efficiency, it could be useful to rewrite the definition of the efficiency. Assuming that the electric power absorbed by the pump is negligible, the efficiency is [17]:

$$\eta_{cycle} = \eta_{el,expander} \cdot \frac{h_3 - h_2}{h_2 - h_1} \quad (5.16)$$

It can be noticed that since the over-heating and the sub cooling are constant, the cycle efficiency is dependent only on the evaporating pressure and the condensing temperature of the working fluid.

Varying these two parameters in a range of [5,15] bar for the evaporating pressure and [40;90] °C for the condensing temperature, it is possible to evaluate the trend of the efficiency as a function of these two factors, as it can be seen in Figure 57.

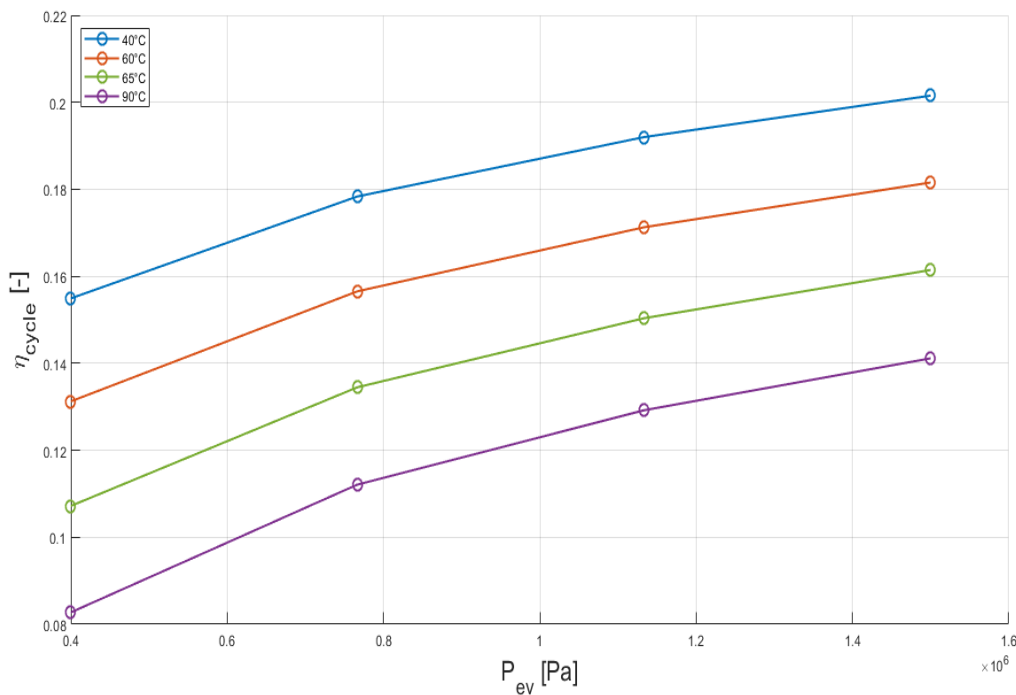


Figure 57 Efficiency of the Rankine cycle vs Evaporating Pressure vs Condensing Temperature

The cycle efficiency increase as the evaporating pressure P_{ev} increase and as the condensing temperature decrease T_{cd} .

To maximize it the Rankine Cycle should work at a P_{ev} equal to 15 bar, that correspond to the limiting pressure of the heat exchanger, while the T_{cd} should be as low as possible.

In general, lowest is the condensing temperature, higher is also the cost of the condenser. This is due to the fact that more the condensing pressure goes under the pressure of 1 bar, non-condensable gas could enter the piping and deteriorate the performance.

5.3.2 Electric and Thermal power produced

The electric power produced in a Rankine cycle, as seen in eq. (5.10), depends on the evaporating pressure, the condensing temperature and the mass flow rate of the working fluid.

As it is for the cycle efficiency, the electric power produced is higher if the evaporating pressure is higher and the condensing temperature is lower.

The water mass flow rate is linked to the values of the supply temperature and the mass flow rate of the heat source of the evaporator.

Assuming a constant evaporating pressure and over-heating, the water mass flow rate increases if the supply temperature or the exhaust gas mass flow rate increase.

Consequently, since the electric power is directly proportional to the water mass flow rate, it is proportional to both the supply temperature and the mass flow rate of the gases.

This trend is shown in Figure 58, where the supply temperature is varied in a range of [220;350] °C and the gas mass flow rate in a range of [1.5;7.5] kg/s.

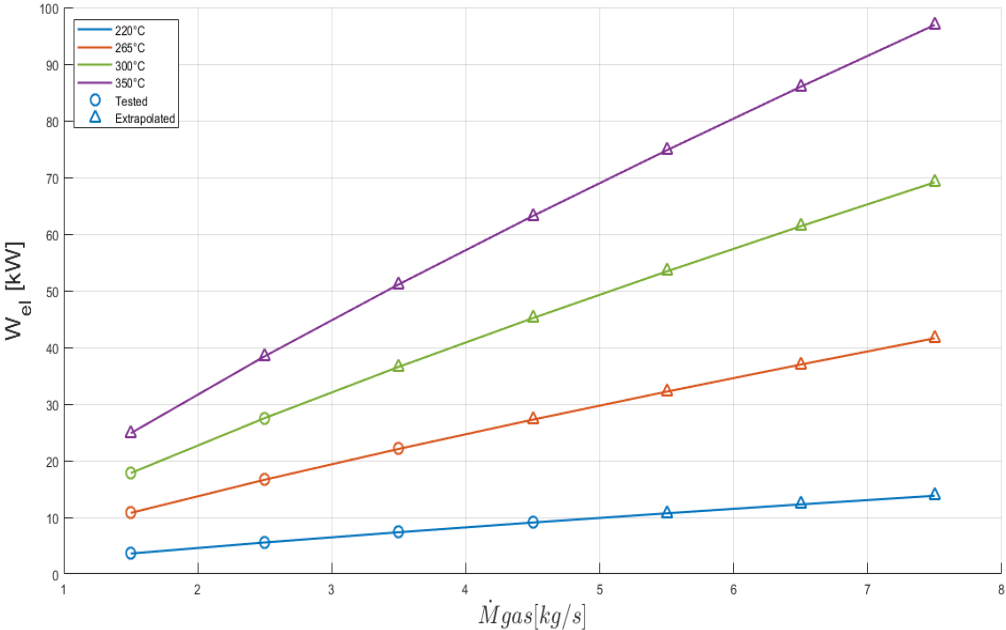


Figure 58 Electric power produced vs Gas mass flow rate vs Gas supply temperature

In Figure 58 the points with the circular marker represent a working condition tested, while the ones with the triangular markers have been extrapolated from the heat exchanger model.

The electric power produced is directly proportional to the gas mass flow rate with a linear law.

This plot is useful to perform a first estimation on the power produced by the Rankine cycle at a given inlet conditions of the gas in terms of gas mass flow rate and supply temperature. As seen in the Table 1 (Section 1.2), the inlet condition of the exhaust gases for some type of aeronautic engines were given from CENCO company.

In the next section the previous analysis is applied to a real case study in order to evaluate the performances of a Rankine Cycle using the exhaust gas of a specific aircraft engine test bench.

5.3.3 Case study: Rygge site

Rygge test bench is located in the airport area of Rygge in Norway and is usually used for the maintenance of military turbojet engines.

Types of tested engines:

Pratt & Whitney F100-220

Location:

Europe, Norway, Rygge

Year of data for building consumption and test hours:

2016

Hours of tests for 2016:

29 motors have been tested during 2016 (110000 litres of fuel consumed). A test duration is comprised between 4 and 6 hours.

The inlet condition of the exhaust gases at the heat exchanger are the ones of the type “standard” tube Turbojet engine presented in Table 1 (Section 1.2):

- Gas mass flow rate: 275,5 kg/s
- Gas supply temperature: 298 °C

With such inlet condition it is possible to do the hypothesis of a parallel connection of multiple heat exchangers.

The exhaust gas mass flow rate intercepted by one heat exchanger depends on the cross section of the duct it is flowing in. In this case the chimney as a rectangular section 4 m x 3 m (CS_{chimney}).

The mass flow rate passing through one heat exchanger is equal to:

$$\dot{m}_{HEX} = \frac{CS_{HEX}}{CS_{chimney}} \cdot \dot{m}_{gas,total} \quad (5.17)$$

In this case the mass flow rate intercepted by one heat exchanger is equal to 3.49 kg/s.

In this condition the electric power produced by the one heat exchanger is 42 kWel. As discussed in the Introduction (Section 1.2), only half of the gas mass flow rate is at the highest temperature (in this case 298°C), so if this is exploited by a series of heat exchanger the electric power produced raises to 1.64 MWel.

If the condensing temperature of the cycle is below the 60°C, there is the possibility of exploiting the condenser as a hot source to heat the buildings of the client.

This would lead, coupled with a storage tank, to a non-negligible save in terms of fuel for the boiler and so in money saved.

5.4 Conclusions

In this chapter a Rankine Cycle model that exploits the calibrated model of the heat exchanger is presented, discussed and analyzed varying the main parameters.

In the light of the results of the efficiency and the electric power calculation, the recovery of the waste heat from a case study shows the promising potential of this technology solution.

6 Conclusions and future work

6.1 Introduction

In this section the objectives of the thesis about the experimental results, the heat exchanger model and the integration of the model in a Rankine Cycle achieved will be explained.

Then recommendations for future research activities about this project will be presented-

6.2 Main objectives and findings of the present study

In the context of the GREEN project presented in the Introduction, one of the objectives of this thesis was the testing of a plate heat exchanger for waste heat recovery.

The experimental facility assembled is able to test the device in a large range of operating condition in terms of gas supply temperature and mass flow rate.

The experimental campaign was made in order to analyze the thermal and hydraulic performance of the device to produce hot liquid water for heating purposes and superheated vapor for electricity production.

As presented in the Chapter 3, the performances of the heat exchanger are promising in terms of low pressure drop on both the water and the gas side.

The pressure drop on the water side are so low to be considered negligible for the Rankine Cycle application, since it does not affect the thermodynamic condition of the working fluid.

On the gas side, to have pressure drop as low as possible (~ 10000 Pa) was an explicit request of the client. The heat exchanger has been proven through the experimental campaign to be able to fully satisfy this important requirement.

A numerical model based on calibrated correlation for the heat transfer and pressure drop has been implemented. It is able to predict the thermal power exchanged and the pressure drop experienced by the two fluid with a relatively small percentage error.

The model is useful to give a first evaluation about the capability of the heat exchanger to recover waste heat from an aircraft engine test bench to produce electricity by means of a steam Rankine Cycle.

The optimal working condition of the Rankine Cycle, taking into account the technical limits of the heat exchanger and the cycle, have been analysed and discussed.

Applying this calculation to a real case study in the Chapter 4, doing the hypothesis of a parallel connection of multiple heat exchanger to exploit the high exhaust gas mass flow rate in the chimney, gives promising results in terms of both electricity and thermal production.

6.3 Recommendations for future work

The numerical model implemented and calibrated in this thesis could be the base of future work about the modeling of this heat exchanger.

In particular transient phenomena appears during the experimental tests especially in the Evaporator mode. A model able to predict the transient performances of the heat exchanger represents an important step for the optimization of a Rankine Cycle where changes of the operating condition can happen frequently.

In order to evaluate the feasibility of a steam Rankine Cycle a techno-economic analysis should be performed.

This analysis will need more precise data about the number of hours tests per year. This data is important since it can indicate an order of magnitude about the possibility of revues from the sale of electricity.

Another consideration to take into account is the possibility of generating electricity at the peak hour demand.

Since the aircraft engine tests lasts at least 4 hours and the time of start depends only on the client, it could be possible to decide to launch the tests when the price of electricity is higher during the day.

7 Bibliography

- [1] R. C. O. D. G. G. e. C. L. A. Barbotin, "Performance enhancement of reheating furnaces using oxycombustion," Chicago, 2000.
- [2] D. A. e. R. V. A. Foresti, "ORCs in steel and metal making industries: lesson from operating experience and next steps," Dusseldorf, Germany, 2015.
- [3] G. Bonvicini, Heat recovery potentials in the most demanding processes.
- [4] [Online]. Available: <http://www.joules-project.eu>. [Accessed 21th October 2018].
- [5] G. L. ,, D. M. ,, Z. H. a. L. V. Legros Arnaud, "Comparison and Impact of Waste Heat Recovery Technologies on Passenger Car Fuel Consumption in a Normalized Driving Cycle," *Energies*, 2014.
- [6] C. F., "Techno-economic and experimental investigation of waste heat recovery from airplane engines test benches," 2018.
- [7] ACTE, [Online]. Available: <http://www.acte-sa.be>. [Accessed 22 09 2018].
- [8] A. 51-1999, Laboratory methods of Testing Fans for Aerodynamic Performance Rating.
- [9] M. G. E. C. A. G. P. C. Tiemo Mathijssen, "Wave speed measurements in non-ideal compressible flows," 2015.
- [10] S. Q. ,, E. G. ,, J. E. B. ,, E. A. G. Ian H. Bell, "A generalized moving-boundary algorithm to predict the heat transfer," *Applied Energy*, 2014.
- [11] D. D. F.P. Incropera, Fundamentals of Heat and Mass Transfer, fifth ed., 2002.
- [12] R. Brent, "Algorithms for Minimization Without Derivatives," *Prentice-Hall*, 1973.
- [13] Z. H. Ayub, "Plate Heat Exchanger Literature Survey and New Heat Transfer and Pressure Drop Correlations for Refrigerant Evaporators," *Heat Transfer*, 2003.
- [14] R. U. T. B. D.-R. K. Wanniarachchi SA, "Approximate correlations for chevron-type plate heat exchangers," pp. 145-1, 1995.

- [15] L. K. K. Y. Han DH, "The characteristics of condensation in brazed plate heat exchangers with different chevorn angles," 2003.
- [16] I. Idel'chik, Handbook of hydraulic resistance, 1966.
- [17] Y. A. B. M. A. Çengel, Thermodynamics: An Engineering Approach, 8th edition, 2015.